Appendices

Appendix 1

A1 Additional geological data for the Wadi Kid area, Sinai, Egypt

Abstract

New data from the Wadi Kid Complex show that the low-angle shear zone, described in detail in chapter, was formed at ~ 595 Ma. Geochemical data from undeformed plutonic and volcanic rocks are comparable to those observed in A-type granites and other late orogenic rocks in other parts of the ANS. These igneous rocks were interpreted to have been derived from mantle magmas in a thinned and extending crust. Shear zones in the upper-crustal rocks display normal movement with top-to-NW movement. These newly obtained data confirm the core complex model for the Wadi Kid Complex that was presented in Chapter 5.

A1.1 Introduction

After the publication of Chapter 5 as a peer-reviewed paper in *Geologie en Mijnbouw* (Blasband et al., 1997), additional research was performed in the Wadi Kid Complex. It was decided to maintain the integrity of this paper for the purpose of future reference. The results of additional research in the form of new relevant field-data, geochronological and geochemical data, will be presented in this appendix.

A1.2 Geological background

In order to present the newly obtained data in this Appendix, the rock-section of the Wadi Kid area was divided in a lower-crustal sequence consisting of metavolcanic and metasedimentary schists of amphibolite grade, foliated and gneissic diorites, tonalites and granodiorites, and an upper-crustal sequence consisting of weakly metamorphosed (lower-greenschist grade) to non-metamorphosed sedimentary and volcanic units (Figure A.1-1). The lower-crustal unit includes the Umm Zariq Fm., Malhaq Fm., Qenaia Fm. and the high grade part of the Heib Fm., which were all described in chapter 5 of this thesis. The upper-crustal rocks, only found in the SE part of the Wadi Kid area, include sandstones, claystones, conglomerates, andesites, basalts and agglomerates. The upper-crustal unit includes the low grade part of the Heib Fm. and the Tarr Fm. which were described in detail in chapter 5. During detailed research that was performed after the publication of Blasband et al. (1997), locally, 50 to 100 m thick bands of chlorite- and biotite-schists, striking NE-SW, were observed within the low-grade metamorphic rocks in the southeastern Wadi Kid Complex. These schists are foliated equivalents of their neighboring rocks, the low-grade metavolcanics and metasediments (Figure A.1-1 and Figure A.1-3b). It was observed that the contact between the lower- and upper-crustal rocks is marked by a brittle cataclastic layer (ca. 0.5 m thick), overlying a chlorite-schist, at the southeastern contact of these units, and a post-Oligocene brittle fault at the northeastern contact of these two units. During the recent research, it was also observed that undeformed and non-metamorphosed rhyolites and ignimbrites overlie all other low-grade rocks in SE part of the Wadi Kid
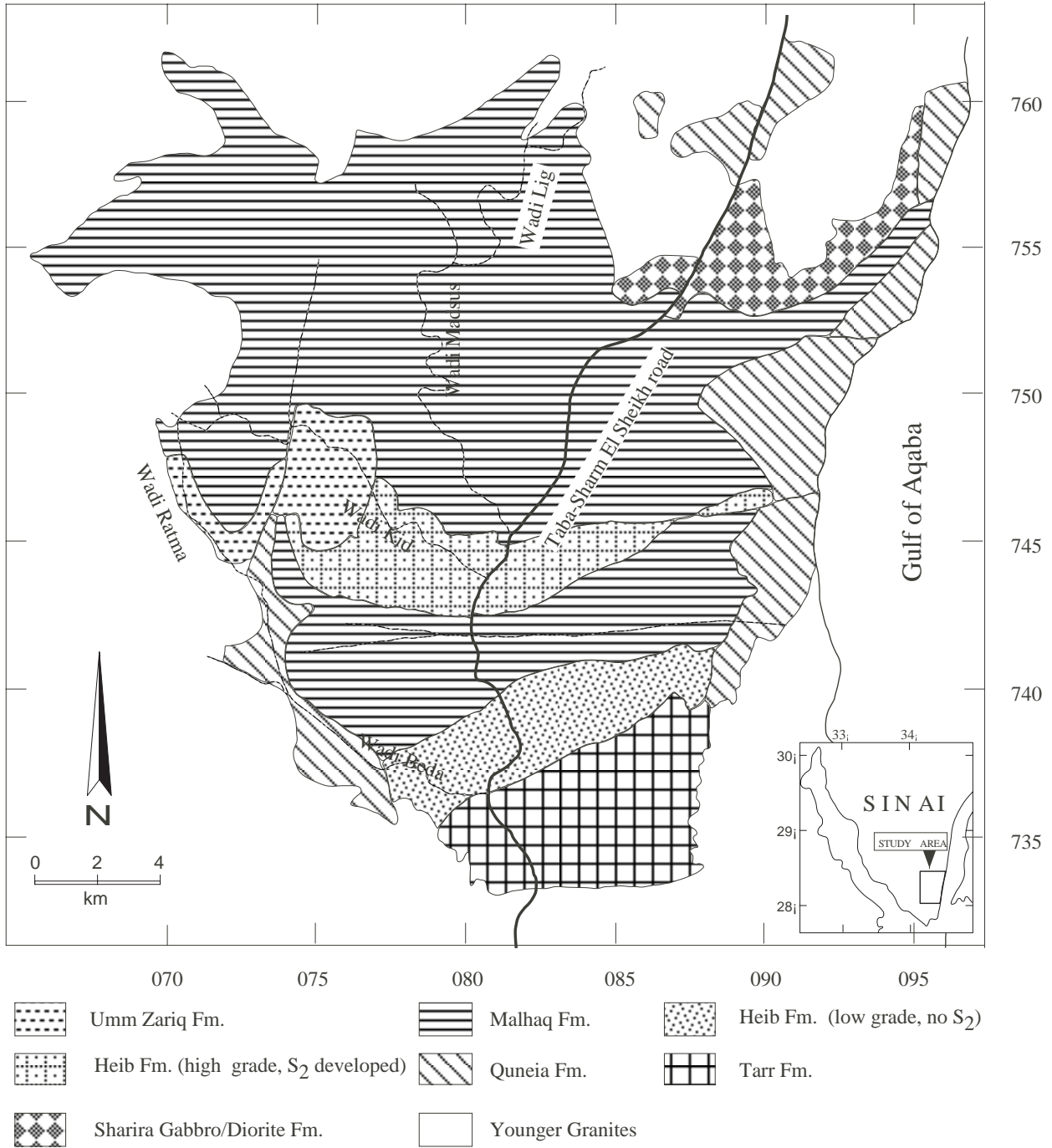
Figure A.1-1 Map of the Wadi Kid Complex presents newly obtained geological data.

Complex..

Brooijmans et al. (2003) postulated two main metamorphic phases: the M1-phase that was responsible for the greenschist grade that was observed in the upper-crustal rocks in the SE part of the Wadi Kid Complex; the M2-phase was responsible for the low-pressure/high-temperature amphibolite grade metamorphism that was observed in the lower-crustal schists.

Structural research that was performed after the publication of Blasband et al. (1997) showed that the oldest deformation phase (D1) in the Wadi Kid area is represented by an S1-foliation that was formed in the greenschist-grade metasedimentary rocks of the southern Wadi Kid area, during M1. This foliation is axial planar to isoclinal F1-folds with NNE-SSW to NE-SW trending fold axes (Figure A.1-1 and Figure A.1-3a). The D1-deformational phase, responsible for the formation of S1 and F1, indicates regional WNW-ESE to NW-SE shortening. In view of the tectonic development of other parts of the ANS and the parallelism of the shortening in the Wadi Kid area to the compressional regime in the Neoproterozoic rocks of NW Saudi Arabia (Stoeser and Camp 1985; Quick 1991), this phase is attributed to arc-

a
N = 35
Contour Interval = 2%
Max. Density = 6.9

b
N = 26
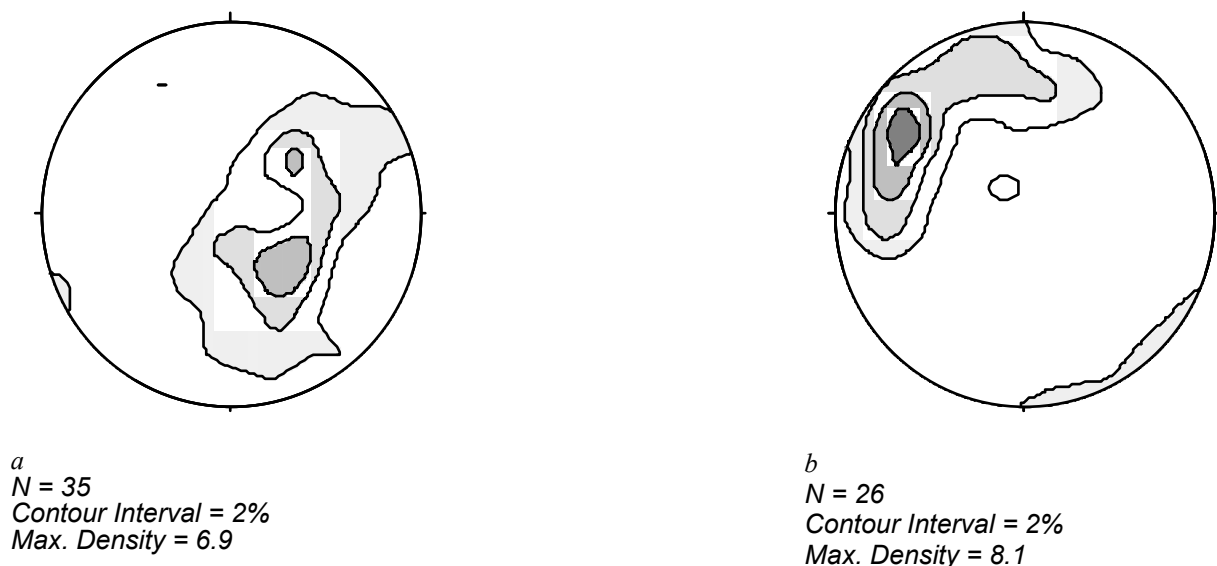*Contour Interval = 2%*
Max. Density = 8.1

Figure A.1-2 (a) Contoured stereographic plot (equal area) of the poles to the S2 foliation in the upper-crustal rocks. (b) Contoured stereographic plot (equal area) of the poles to the L2 lineation in upper-crustal rocks, showing maximum at NW.

accretion with a WNW-ENE to NW-SE compressional stress field.

The D2-phase is mainly represented by the deformation features in the lower-crustal rocks. These have been described in detail in chapter 5. The S2-foliation is subhorizontal and best developed in the amphibolite-grade schists (see Chapter 5). A NW-SE trending mineral and stretching lineation is developed on the S2-foliation (Figure 5-5 in Chapter 5). A large variety of indicators of non-coaxial strain have been described in Chapter 5 and they indicate a main phase of top-to- NW movement that was followed by shear reversal and a top-to-SE movement (see Chapter 5). Recent research shows that the thin chlorite- and biotite-schists that cross-cut the upper-crustal greenschist-grade rocks represent D2 features in the upper-crustal

a

b
Figure A.1-3 (a) F1-folds, folding a S0-bedding, and S1-foliation in the low-grade metasediments of the SE Wadi Kid area. (b) NE-SW striking chlorite-schist in the SE Wadi Kid, representing splays off the deeper shear in the upper-crustal rocks. Extensional crenulation cleavages indicate dextral movement (in this case top-to-the-NW).

section (Figure A.1-1). Asymmetric features as extensional crenulation cleavages (Figure A.1-3b), indicate that these moderately NW dipping mylonitic zones (Figure A.1-2a), with a NW plunging lineation (Figure A.1-2b), all display a top-to-the-NW-movement.

The Wadi Kid area is cross-cut by NE-SW trending mafic, felsic and composite dykes. The mineral and stretching lineations are orthogonal to the strike of the dykes and the fact that these two features are synchronous, indicate NW-SE extension (See Chapter 5).

A1.3 Geochemistry of undeformed igneous rocks in the Wadi Kid Complex

A1.3.1 Introduction

Geochemical studies may proof useful in discriminating between magmatic processes and tectonic regimes and have been widely used for tectonic interpretations in the Arabian-Nubian Shield (e.g. Brown et al., 1989; Hassanen, 1996; Jarrar et al, 2003). In this appendix, the results of the major element and trace element analyses for undeformed key-samples from the Wadi Kid Complex were compared with those of other trace element studies in the Arabian-Nubian Shield and other areas. The methods for the geochemical analyses were identical to those that were used for the analyses of the samples from the Tabalah/Tarj area. These methods were described in Chapter 4 of this thesis.

A1.3.2 Samples

Five samples, that are representative for the undeformed igneous rocks from Wadi Kid Complex, were analyzed for geochemical studies through ICP-MS. These samples are:

- A *basalt* from a mafic dyke in the central Wadi Kid Complex area that trends 40˚. This type of dyke is often found cross-cutting the undeformed granites and was related to the later stage of extension in Wadi Kid Complex.

- A *rhyolitic rock* from a felsic dyke from the central Wadi Kid Complex area that trends 45˚. This type of dyke is often found cross-cutting the undeformed granites and was related to the later stage of extension in Wadi Kid Complex. Similar dykes, near the Wadi Kid area, were dated at 620-560 Ma (Stern & Manton 1987).

- An *undeformed granite* from the northern Wadi Kid Complex. These granites rocks were dated at 590–530 Ma (Bielski, 1982) and intrude the lower crustal schists and thus also represent a relict of the later stages in the Wadi Kid Complex

- A *massive rhyolite* that overlies the greenschist grade schist in the southern Wadi Kid Complex. Similar rhyolites in southwest Jordan were dated at 553 Ma (Jarrar *et al.* 1992).

- An *underformed basaltic flow* that overlies the greenschist grade schist in the southern Wadi Kid Complex

A1.3.3 Results

The results of the major-element analysis are shown in Table A.1-1 and the results for the trace element analyses are shown in Table A.1-2. The N-MORB normalized diagrams in Figure A.1-4 and the REE chondrite-normalized diagrams in Figure A.1-5 justify the division into 2 groups of the samples from the Wadi Kid Complex:

   I) The mafic rocks: The basaltic dyke and the basalt flow
   II) The felsic rocks: the alkali- granite, the rhyolitic dyke and the massive rhyolite

   Generally, the relative young and undeformed granites in the Arabian Nubian Shield were interpreted to be late- or post-orogenic A-type granites (Kuster and Harms, 1998). The

Table A.1-1 Major element analyses for the analyzed samples from the Wadi Kid Complex

Sample	Basalt	Massive rhyolite	Rhyolitic dyke	Undeformed granite	Basaltic dyke
Na2O	4,22	4,48	4,54	4,29	3,23
MgO	2,19	0,456	0,456	0,718	6,61
Al2O3	15,8	13,6	13,8	13,7	14,9
SiO2	61,9	70,1	71,3	69,5	44,6
P2O5	0,292	0,127	0,122	0,188	0,373
K2O	2,41	4,62	4,64	4,59	0,599
CaO	4,87	1,27	1,27	1,66	8,49
TiO2	0,842	0,582	0,591	0,588	1,89
MnO	0,088	0,072	0,074	0,081	0,143
Fe2O3	5,74	3,6	3,85	3,84	13,3

major elements for the undeformed granite, the rhyolitic dyke and the massive rhyolite in the Wadi Kid Complex display the geochemical characteristics of A-type alkaline granites, with concentrations of SiO2 ≈ 70%, Na2O + K2O > 7 and CaO < 1.8 (see also table Table A.1-1). These concentrations are typical for rocks with an A-type granite geochemistry (Nelson Eby, 1990). The felsic rocks in the Wadi Kid Complex also display trace-element patterns which characterize A-type granites in other parts of the Arabian Nubian Shield as in eastern Egypt (Hassanen, 1996), southwestern Jordan (Jarrar et al, 2003), southern Israel (Kessel et al., 1998) and Sudan (Kuster and Harms, 1998). In these areas, N-MORB normalized diagrams display an enrichment of the LFS-elements relative to the HFS-elements with a pronounced Sr trough; REE-diagrams display enrichment relative to HREE with pronounced negative Eu-anomaly. These patterns are also observed in the Wadi Kid Complex (Figure A.1-4 and Figure A.1-5). Through additional Sr-, Nd-, Pb- and O-isotope studies, Beyth et. al. (1994) and Kuster and Harms (1998) showed that the A-type granites in other parts of the Arabian Nubian Shield were derived from a lithospheric mantle and included evidence for partial melting of a continental crust. Likewise, Jarar et al. (2003) and Kessel et al. (1998) postulate that the A-type granites and their related volcanics were derived from mantle magmas which underwent extensive fractional crystallization. This form of magmatism is best explained to take place in thinned lithosphere in the very late stages of or completely after a compressional event and these igneous rocks was thus interpreted to be late- to pos-tectonic (Kuster and Harms, 1998; Sylvester, 1989)

The mafic rocks of the Wadi Kid Complex must be late because the basaltic dykes are observed intruding the undeformed granites. The N-MORB patterns of the mafic rocks are characterized by enrichment of the LFS-elements relative to the HFS-elements but lack anomalies. The REE-patterns for the mafic rocks show an enrichment of LREE relative to HREE but lack the Eu-anomaly observed in the felsic rocks. These geochemical patterns are similar to geochemical patterns observed for late mafic volcanics in southern Israel (Kessel et

Table A.1-2 Trace element analyses for the analyzed samples from the Wadi Kid Complex

Sample	Basaltic dyke	Undeformed granite	Rhyolitic dyke	Massive rhyolite	Basalt
Rb	8,31	109,3	126,9	81,10	71,44
Sr	330,4	139,9	173,8	94,79	1018,20
Y	11,85	31,22	32,76	10,54	22,55
Zr	86,96	107,8	363,5	101,2	220,72
Nb	7,91	28,05	27,26	7,47	11,13
La	10,06	51,90	42,93	22,27	26,83
Ce	23,84	114,7	98,85	49,09	63,42
Pr	3,24	13,43	12,01	5,54	7,83
Nd	13,85	50,85	45,85	19,54	32,10
Sm	3,25	9,39	9,08	3,52	6,70
Eu	1,08	1,46	1,96	0,50	1,93
Gd	3,29	8,18	8,06	2,82	5,89
Tb	0,51	1,21	1,23	0,42	0,85
Dy	2,79	6,63	6,85	2,34	4,72
Ho	0,54	1,24	1,31	0,44	0,90
Er	1,44	3,52	3,70	1,28	2,41
Tm	0,21	0,53	0,58	0,20	0,36
Yb	1,31	3,54	3,69	1,37	2,35
Lu	0,21	0,57	0,59	0,22	0,37
Hf	2,34	3,46	10,00	3,65	5,89
Ta	1,38	3,57	3,30	1,20	1,51
Th	0,81	11,81	8,92	14,55	5,65

al, 1998), Sudan (Kuster and Harms, 1998) and the Dokhan Volcanics in Eastern Egypt (Moghazi, 2003). These authors interpret the mafic rocks to be part of bi-modal mafic/felsic volcanic suites and consequently relate the mafic rocks to the felsic rocks that were discussed in the previous paragraph. Kuster and Harms (1998) suggested that these mafic rocks originated from the lithospheric mantle. This would have happened in a extending and thinning crust (Moghazi, 2003).

It can be concluded that the undeformed igneous rocks in the Wadi Kid Complex resemble late- to post-orogenic igneous rock-suites in other parts of the Arabian-Nubian Shield. These rocks were suggested to have been derived from mantle magmas in a extending and thinning crust.

A1.4 Geochronology: Ar-Ar dating for the main lower-crustal amphibolite

Two key-samples were dated in order to constrain the age of the main tectonic phase in the
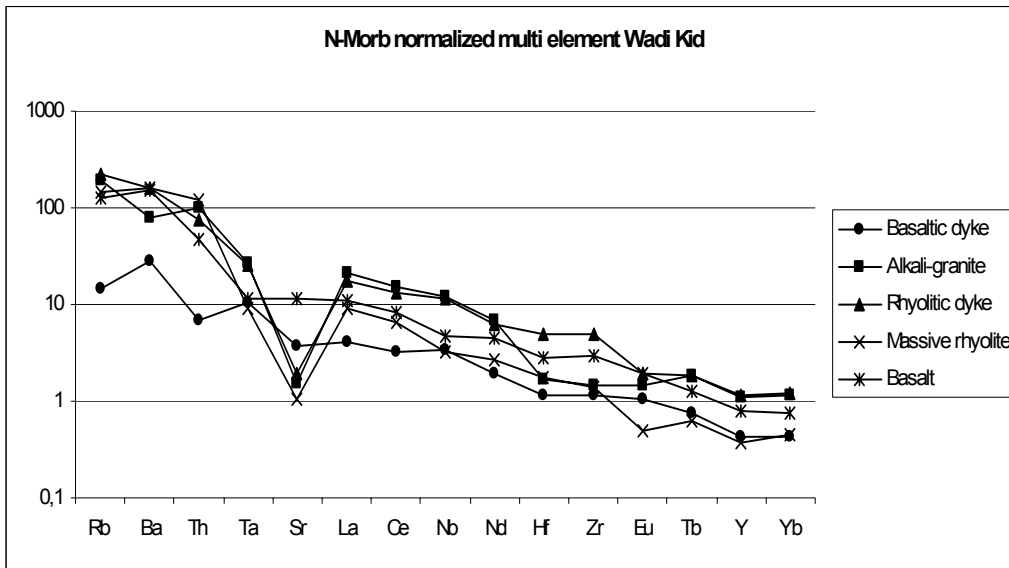
Figure A.1-4 N-MORB normalized multi element diagram for the selected samples from the Wadi Kid Complex.
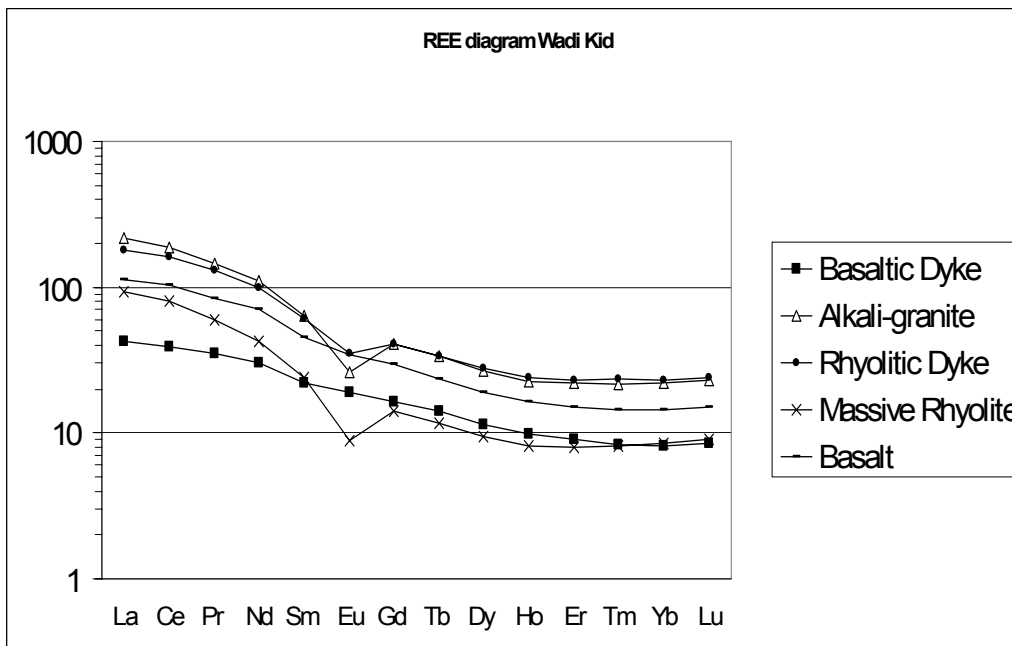

Figure A.1-5 Chondite normalized REE for the selected samples from the Wadi Kid Complex

Wadi Kid Complex, the D2 phase, as identified in Chapter 5. The ^{40}Ar/^{39}Ar-method was chosen for the dating because this allows dating of amphibolite-grade rocks through dating of hornblendes. Furthermore, hornblende has good argon retentivity properties with a closure temperature of 525º C for well crystallized hornblende (McDougall & Harrison, 1999). The hornblendes in the samples define the highest metamorphic grades found in these rock-types so their dates would define the age for the peak tectono-metamorphic event. The method for the geochronological analyses was identical to the one that was used for the analyses of the samples from the Tabalah/Tarj area. This method was described in Chapter 4 of this thesis.
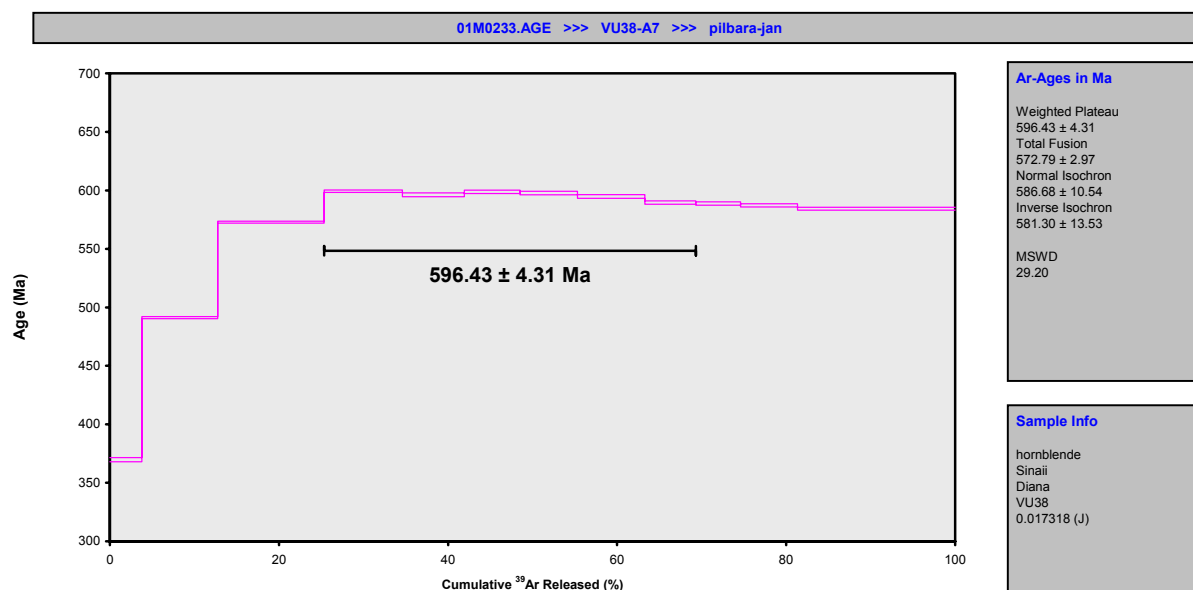
The chosen samples, SIN 1 and SIN 2, are both hornblende schists from the central Wadi Kid Complex (for their location see Figure A.1-1) and display relicts of the D2/M2 phases. The

Table A.1-3a Table with detailed tables of the individual step-heating for the $^{40}Ar/^{39}Ar$ dating of samples SIN 1

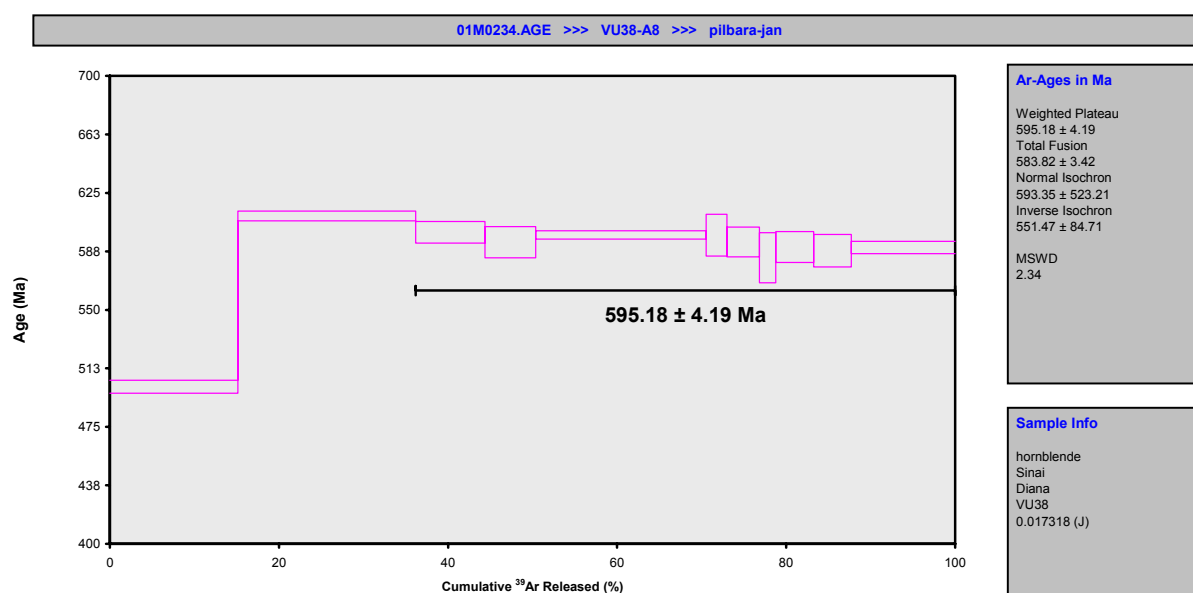**Incremental Heating**

			^{36}Ar(a)	^{37}Ar(ca)	^{38}Ar(cl)	^{39}Ar(k)	^{40}Ar(r)	Age (Ma)	± 2σ	^{40}Ar(r) (%)	^{39}Ar(k) (%)	K/Ca	± 2σ
01M0234A	0,25 W	□	0,00419	0,26863	0,01414	0,63938	11,80944	500.69	± 4.11	90,51	15,14	1,023	± 0,772
01M0234B	0,40 W	□	0,00197	2,16198	0,02393	0,88767	20,62983	610.21	± 3.12	97,25	21,03	0,177	± 0,024
01M0234C	0,45 W	▲	0,00039	1,10876	0,01084	0,34647	7,88950	599.72	± 6.92	98,54	8,21	0,134	± 0,027
01M0234D	0,50 W	▲	0,00029	1,11905	0,00956	0,25307	5,69116	593.38	± 10.00	98,53	5,99	0,097	± 0,020
01M0234F	0,55 W	▲	0,00068	5,42609	0,04203	0,85154	19,32659	598.04	± 2.61	98,96	20,17	0,067	± 0,007
01M0234G	0,58 W	▲	0,00013	0,64596	0,00386	0,10393	2,35782	597.84	± 13.42	98,34	2,46	0,069	± 0,009
01M0234H	0,60 W	▲	0,00017	1,06746	0,00670	0,16175	3,63855	593.54	± 9.55	98,64	3,83	0,065	± 0,007
01M0234I	0,63 W	▲	0,00008	0,47080	0,00303	0,08232	1,81492	583.44	± 16.08	98,78	1,95	0,075	± 0,011
01M0234K	0,70 W	▲	0,00009	1,42096	0,00908	0,18882	4,22029	590.28	± 9.91	99,35	4,47	0,057	± 0,006
01M0234L	0,80 W	▲	0,00014	1,45674	0,00887	0,18800	4,18258	587.95	± 10.45	99,02	4,45	0,055	± 0,006
01M0234M	fsn	▲	0,00040	3,45736	0,02149	0,51888	11,59121	590.01	± 3.97	98,99	12,29	0,065	± 0,007
Σ			0,00852	18,60378	0,15353	4,22184	93,15191						

Results

	^{40}(r)/^{39}(k)	± 2σ	Age (Ma)	± 2σ	MSWD	^{39}Ar(k) (%,n)	K/Ca	± 2σ
Error Plateau	22,5685	± 0,1286 ± 0,57%	595.18	± 4.19 ± 0,70%	2,34	63,83 9	0,064	± 0,007
		External Error		± 12.62				
		Analytical Error		± 2.89				
Total Fusion Age	22,0643	± 0,0735 ± 0,33%	583.82	± 3.42 ± 0,59%		11	0,098	± 0,004
		External Error		± 12.17				
		Analytical Error		± 1.66				

Information on Analysis

Sample	VU38-A8
Material	hornblende
Location	Sinai
Analyst	Diana
Project	pilbara-jan
Irradiation	VU38
J-value	0,017318
Standard	98,3

Appendix 1

Table A.1-3b Table with detailed tables of the individual step-heating for the $^{40}Ar/^{39}Ar$ dating of samples SIN 2

Incremental Heating			$^{36}Ar(a)$	$^{37}Ar(ca)$	$^{38}Ar(cl)$	$^{39}Ar(k)$	$^{40}Ar(r)$	Age (Ma)	± 2σ	$^{40}Ar(r)$ (%)	$^{39}Ar(k)$ (%)	K/Ca	± 2σ
01M0233B	0,25 W	☐	0,01551	0,40049	0,02183	0,97980	12,87070	369.78	± 1.82	73,73	3,77	1,052	± 0,206
01M0233C	0,40 W	☐	0,02031	0,70265	0,03917	2,33704	42,23185	491.20	± 0.87	87,55	8,99	1,430	± 0,163
01M0233D	0,45 W	☐	0,00955	1,93078	0,05404	3,27098	70,58409	572.81	± 0.76	96,15	12,58	0,728	± 0,073
01M0233E	0,50 W	▲	0,00430	2,71273	0,04177	2,40940	54,81894	599.30	± 1.04	97,73	9,27	0,382	± 0,038
01M0233G	0,55 W	▲	0,00223	3,37396	0,03904	1,90634	43,10865	596.19	± 1.59	98,49	7,33	0,243	± 0,024
01M0233H	0,60 W	▲	0,00226	2,68100	0,03159	1,71535	38,98984	598.80	± 1.47	98,31	6,60	0,275	± 0,027
01M0233I	0,65 W	▲	0,00172	4,18352	0,04281	1,76553	40,04563	597.73	± 1.48	98,74	6,79	0,181	± 0,018
01M0233J	0,70 W	▲	0,00242	6,05644	0,05936	2,07375	46,76618	594.80	± 1.61	98,48	7,97	0,147	± 0,015
01M0233L	0,75 W	▲	0,00171	3,04940	0,03242	1,56320	34,89203	589.61	± 1.38	98,57	6,01	0,220	± 0,022
01M0233M	0,80 W	☐	0,00133	2,54626	0,02862	1,37926	30,73382	588.75	± 1.49	98,73	5,30	0,233	± 0,024
01M0233N	0,90 W	☐	0,00191	5,26072	0,04861	1,75462	38,97612	587.19	± 1.36	98,57	6,75	0,143	± 0,014
01M0233O	fusion	☐	0,00771	16,97158	0,11384	4,84798	107,07849	584.34	± 1.19	97,91	18,64	0,123	± 0,012
Σ			0,07095	49,86952	0,55310	26,00327	561,09637						

Results		$40_{(r)}/39_{(k)}$	± 2σ	Age (Ma)	± 2σ	MSWD	$^{39}Ar(k)$ (%,n)	K/Ca	± 2σ
Error Plateau		22,6242	± 0,1356 ± 0,60%	596.43	± 4.31 ± 0,72%	29,20	43,97 6	0,203	± 0,053
				External Error	± 12.68				
				Analytical Error	± 3.05				
Total Fusion Age		21,5779	± 0,0169 ± 0,08%	572.79	± 2.97 ± 0,52%		12	0,224	± 0,009
				External Error	± 11.83				
				Analytical Error	± 0.39				

Information on Analysis

Sample	VU38-A7
Material	hornblende
Location	Sinaii
Analyst	Diana
Project	pilbara-jan
Irradiation	VU38
J-value	0,017318
Standard	98,3

a

b

Figure A.1-6 Age spectra for (a) SIN 1 and (b) SIN 2

rocks contain hornblende, biotite, plagioclase and quartz. The samples were well lineated and foliated. The hornblendes define the lineations. The samples represent the main low-angle shear zone that was described in detail in chapter 5. The age spectra for the analyzed samples from the Wadi Kid Complex areas are shown in Figure A.1-6. The detailed tables of the individual step-heating can be found in table A.1-3. All analyzed samples display clear plateaus with no evidence of a secondary event outside of event that formed the main plateau. The results of $^{40}Ar/^{39}Ar$ dating for sample SIN 1 displays an age of 596 $\pm$ 4 Ma and for SIN 2 an age of 595 $\pm$ 4 Ma (Figure A.1-6). These dates represent the ages of the M2 and D2 phases which formed the low-angle shear zone.

A1.5 Conclusions

This appendix presents new geological data for the Wadi Kid Complex that is additional to the data that was presented in Chapter 5. These new data include the following geological information:

• Undeformed and non-metamorphosed rhyolites and ignimbrites overlie the low-grade deformed rocks. Geochemical data show that these were formed during extension.

• F1-folds with NNE-SSW to NE-SW trending fold axes and a related S1-foliation were formed during the D1-deformational phase. These structures formed during WNW-ESE to NW-SE compression. This trend of compression is also observed in the Later Proterozoic of northwestern Saudi Arabia, where this phase is attributed to arc-accretion (Stoeser & Camp 1985; Quick 1991).

• Moderately NW-dipping shear zones, with a thickness of 50 to 100 m, cross-cut the upper-crustal unit. These shear zones display a top-to-NW sense of shear. This sense of shear is also the initial sense of movement that was observed on the sub-horizontal lower-crustal shear zone that was formed during D2 (see also chapter 5). Therefore I interpret the moderately NW-dipping shear zones in the upper-crustal unit also to have been formed during D2.

• Locally, the contact between the lower- and upper-crustal rocks is marked by a brittle cataclastic layer.

• Geochemical data for the non-deformed igneous rocks, A-type granites, rhyolites and basalts indicate that these were derived mantle magmas that were intruded into a thinned and extending crust.

• The low-angle shear zone in the lower-crustal rocks, formed during D2, was dated at ≈ 595 Ma

An updated section across the Wadi Kid area is shown in Figure A.1-7a and an interpretation is presented in Figure A.1-7b. In this interpretation it is shown that upper-crustal rocks, metavolcanics and metasediments, display the compressional features that are indicative of the D1 -deformation phase. These rocks structurally overlie lower-crustal rocks, mainly mylonites, in the form of amphibolites and metaplutonic rocks, which were formed in an NW-SE extensional regime during the D2 -deformation phase (see also chapter 5). These shear zones were dated at ≈ 595 Ma.

The NE-SW striking shear zones in the upper-crustal metamorphics are interpreted as original splays off the deeper shear and were also formed during the extensional D2-phase. The lower- and upper-crustal rocks are separated by a brittle shear. Undeformed A-type granites intruded the lower-crustal mylonitic sequence. Geochemical studies show that these are alkaline granites that were derived through fractional crystallization from mantle magmas. This happened in a thinned and extended crust. The basaltic and felsic dykes, and the undeformed rhyolites and and undeformed basalts that overlie overlie the upper-crustal deformed rocks, were also derived from the same mantle magmas. In chapter 5, it is suggested that the SE-sense of movement in the lower-crustal mylonitic sequence postdated the NW-sense of movement and that this reversal was a result of doming. A cataclasite separates the lower- and upper-crustal units.
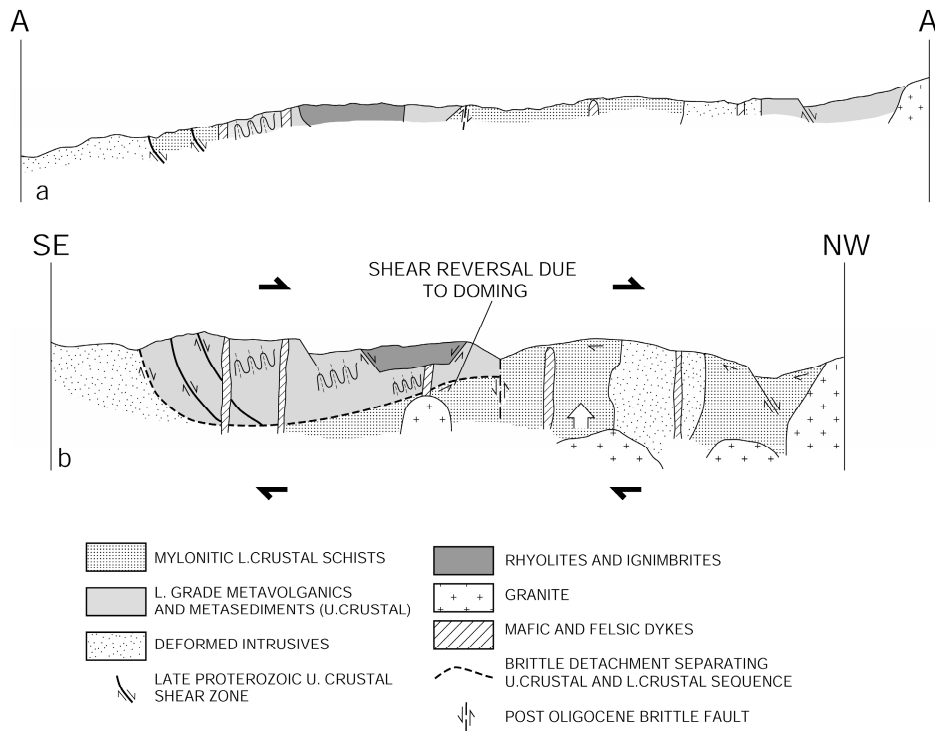
Figure A.1-7 Schematic cross-section through the Wadi Kid (section A-A' in Figure A.1-1)

The newly presented data in this appendix confirm the core-complex model for the Wadi Kid Complex that was presented in chapter 5. The sequence consisting of deformed plutons, of thick subhorizontal amphibolite-grade schists with uniformly trending lineations (described in detail in chapter 5), and which were formed at HT/LP conditions in an extensional regime, overlain by rocks displaying relics of older compressional phases, with a cataclasite separating the two sequences.

A.2 Geothermobarometric evidence for a metamorphic core-complex in Sinai, Egypt

Abstract

Blasband et al. (1997, 2000) postulated a metamorphic core complex model for the Wadi Kid area, south Sinai, Egypt. This core complex was formed in an extensional setting after gravitational collapse of the East African Orogen in the Late Proterozoic. Arc-accretion was responsible for the closure of the Mozambique Ocean. Blasband et al (1997, 2000) based their theory mainly on structural data. In order to justify this model geothermobarometric evidence is crucial. Therefore the metamorphic rocks of the Wadi Kid area were the subject of a detailed metamorphic study.

The M_1 metamorphic phase is characterized by greenschist facies conditions and is related to arc-accretion. The M_2 metamorphic phase is the main subject of this paper. The petrologic characteristics of pelitic and mafic rocks that were metamorphosed during M_2 show that the lower crustal rocks in the Wadi Kid area were subjected to upper-greenschist to upper-amphibolite conditions of the low-pressure/high-temperature type at the end of the Late Proterozoic. Garnet-biotite and amphibole-plagioclase geothermometry reveal temperatures of 488-684 °C. Plagioclase-biotite-muscovite-garnet geothermometry and amphibole-plagioclase geobarometry indicate pressures of 3.42-4.28 kbar.

The M_2 metamorphic phase is associated with a D_2 deformation phase. This phase is a relict of gravitational collapse during the final stages of the collision of East and West Gondwanaland.

A.2.1 Introduction

Blasband et al. (1997) were the first to acknowledge the presence of core complexes in the Arabian Nubian Shield, more specifically the Wadi Kid area (S.E. Sinai, Egypt). Structural studies in this area indicated the presence of a core complex as a result of extensional collapse during the Late Proterozoic (Blasband et al. 1997, 2000). Because core complexes display a typical metamorphic evolution, we believe that a detailed metamorphic study is necessary to demonstrate that the core complex model is valid for the Wadi Kid area.

Previous studies in the Wadi Kid area indicate that two metamorphic phases can be recognized (Shimron 1980, 1984, 1987; Reymer 1983, 1984a, 1984b). Phase M_1 is characterized by greenschist facies conditions (Shimron, 1987). Pressure and temperature conditions were estimated at 3-4 kbar and 300-400 °C. The M_1 phase was believed to have been

related to compression at upper crustal levels (Reymer, 1983, 1984a; Shimron, 1980, 1984, 1987) The M_2 phase is associated with deformation phase D_2 (Blasband et al., 1997, 2000). Studies by Reymer et al. (1984) and Shimron (1987) indicate upper-amphibolite facies conditions for this phase.

The aim of this research was to study and re-evaluate the metamorphic evolution of the Wadi Kid area and the metamorphic conditions in the lower crustal rocks in particular on the basis of new geothermobarometric data from the metapelitic and metavolcanic rocks of the Wadi Kid area.

This study indicates that the M_1 stage of greenschist-facies metamorphism was associated with a phase of arc-accretion. The M_2 stage of high-temperature/low-pressure type was associated with extension and the subsequent intrusion of large volumes of granitoids. The temperatures were between 488-684 °C and pressures between 3.42 kbar and 4.23 kbar respectively. The M_2 metamorphism is Furthermore we show that the metamorphic petrology and the geothermobarometric data support the core complex model for the Wadi Kid area as described by Blasband et al. (1997, 2000).

A.2.2 Lithology

The Wadi Kid area consists of low- to high-grade metamorphic rocks and plutonic rocks of Late Proterozoic age which have been described and discussed by Shimron (1980, 1983, 1984), Furnes et al. (1985), and Reymer (1983, 1984a). The distribution of these rocks in the Wadi Kid Area is shown in Figure A.2-1. The Malhaq Fm., Umm Zariq Fm., the Heib Fm., and the Tarr Fm. represent the metamorphic sequence. The total thickness of this sequence is estimated to be 1.5 km. The Quneia Fm., the Sharira Diorite, and alkaline granites represent the (meta-) plutonics. Dikes crosscut all formations.

The *Umm Zariq Fm.* is a sequence of meta-pelites and meta-psammites. Within the Umm Zariq Fm., relict sedimentary structures, such as bedding, cross-bedding, slump structures and fining upward sequences are found in the less schistose lenses.

The strongly foliated metapelites contain fine-grained biotite, muscovite, (retrograde) chlorite, plagioclase and K-feldspar along with porphyroblasts of garnet, andalusite, staurolite, biotite and cordierite. The foliation is defined by biotite and muscovite flakes and flattened quartz grains. Garnets are present as anhedral and subhedral crystals between 0.3 and 2.4 mm in diameter. They contain only few inclusions of quartz, plagioclase, K-feldspar and ilmenite. Inclusion trails are absent. Staurolites occur as anhedral porphyroblasts up to 3.5 mm. Biotite, muscovite and quartz (Figure A.2-2) partly replace them. Andalusite porphyroblasts are anhedral, up to 4 mm and are locally replaced by biotite or muscovite (Figure A.2-3). Andalusites with inclusion trails were found in the Wadi Umm Zariq. Chiastolite is common and shows re-entrant zones with feather structures and growth inclusions. Inclusions in the chiastolite consist of biotite, quartz and ilmenite. Cordierite porphyroblasts are spherical, up to 5 mm in size and show sector twinning. Inclusions are numerous and consist of groundmass components.

The *Malhaq Fm.* is a metavolcanic sequence (Furnes et al., 1985) of biotite-schists and minor amounts of fine-grained, less-deformed, massive, metamorphosed volcanics. The biotite-
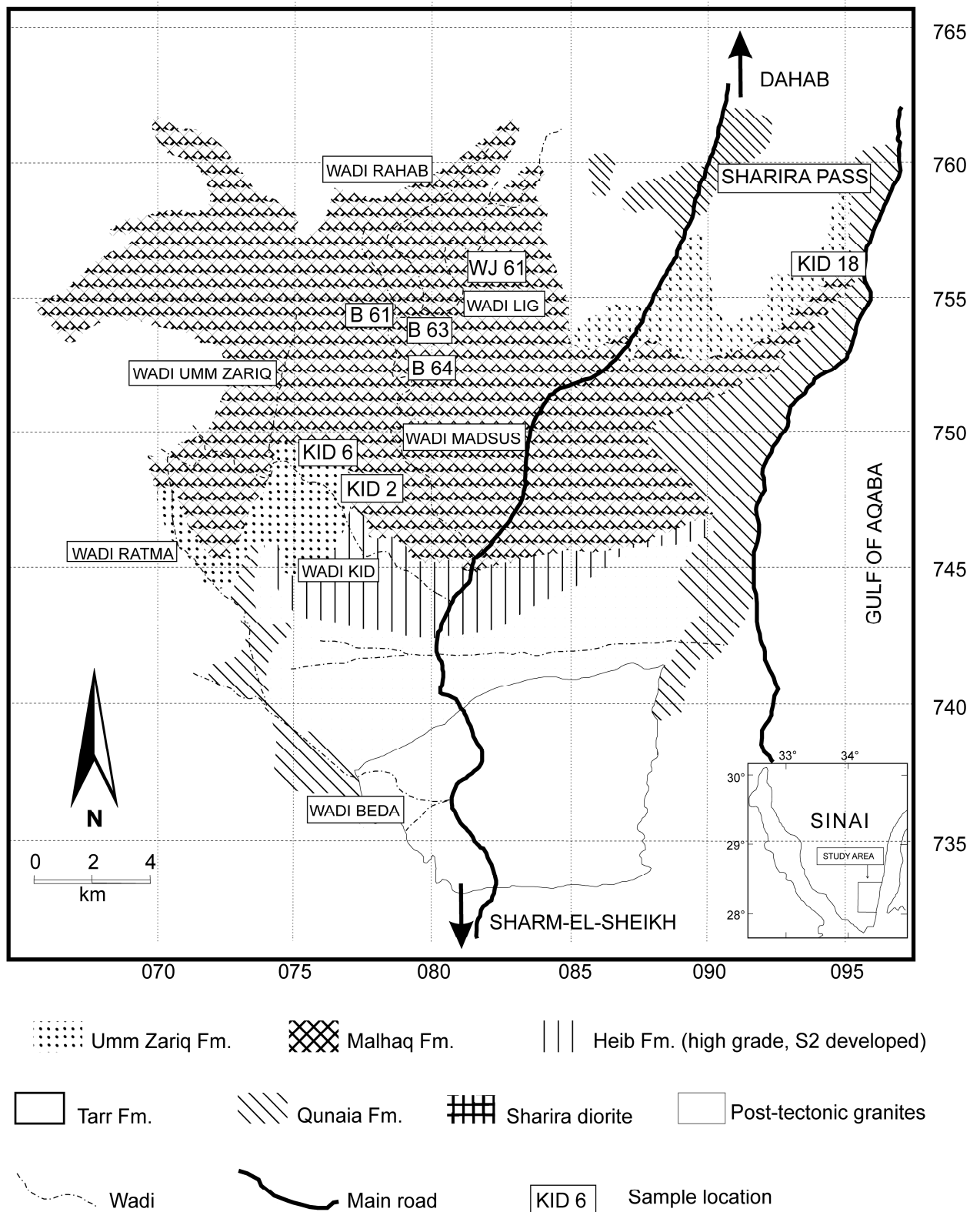
Figure A.2-1 Map of the Wadi Kid belt with an outline of the geological units and sample locations (modified after Shimron, 1987 and Blasband et al., 1997).
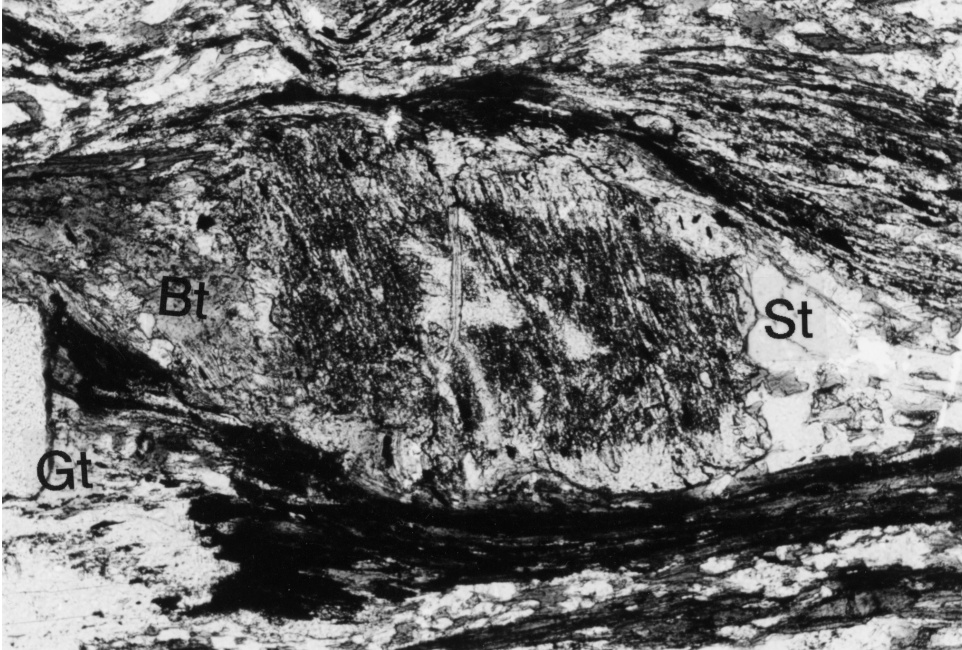
Figure A.2-2 Staurolite porphyroblasts in sample Kid 6, a pelitic schist from the Umm Zariq Fm., with in the left

schists contain feldspar, quartz, biotite and hornblende. Hornblende, biotite, flattened quartz and minor chlorite define the schistosity in the rocks of the Malhaq Fm. The massive equivalents of these schists occur as layers and blocks within the schists and contain biotite, muscovite, chlorite, some quartz and K-feldspar. Garnet, andalusite and staurolite are also present, as porphyroblasts in the Malhaq Fm. Quartz is present as flattened grains, which display undulatory extinction. Chlorite is brown to colorless. Staurolite porphyroblasts show mutual contacts with muscovite, andalusite and feldspar, and are partially replaced by muscovite. Anhedral andalusite porphyroblasts are up to 5 mm in size and contain inclusions of
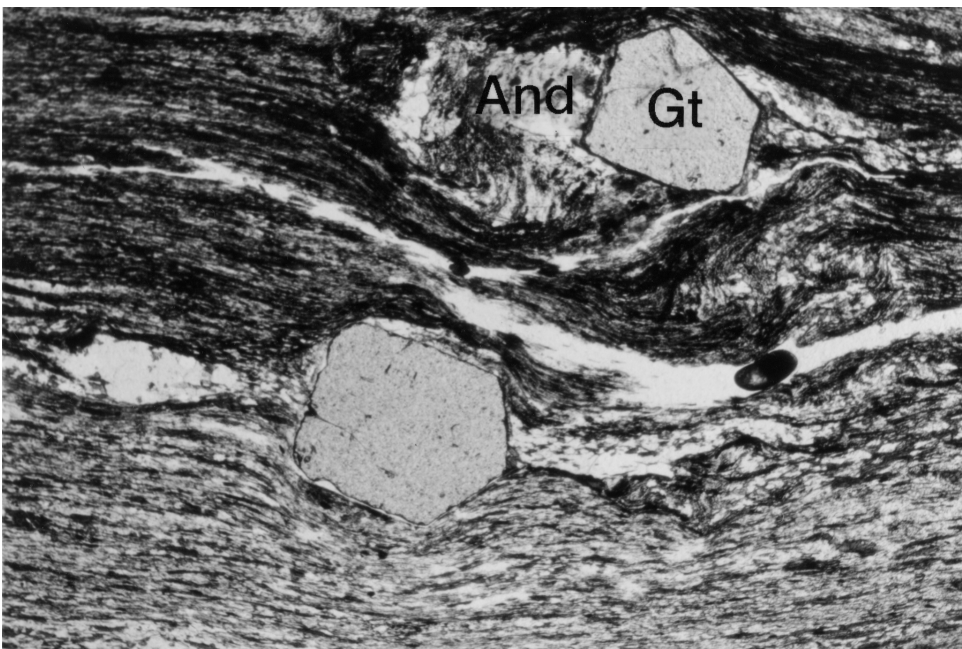
Figure A.2-3 Garnet in mutual contact with andalusite in sample Kid 6, Umm Zariq Fm.. Garnet and biotite are replacing andalusite. Magnification 30x.
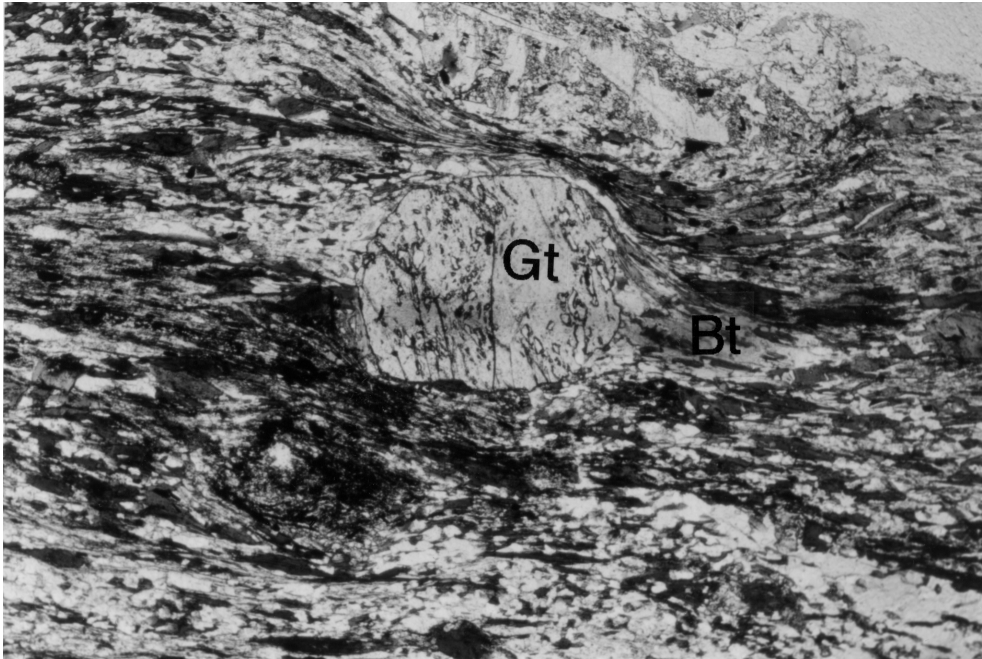
Figure A.2-4 Garnet in sample Kid 18, Malhaq FM., enclosed by muscovite, plagioclase and quartz. Pressure shadows on the edges are clearly visible. Magnification 30x.

quartz, plagioclase, garnet and ilmenite. No clear inclusion trails are observed in the andalusites. The andalusites are partially replaced by biotite and muscovite. Anhedral and subhedral garnet porphyroblasts with irregularly shaped rims are up to 1.4 mm in size (Figure A.2-4). The inclusions in the garnets consist of plagioclase, quartz and ilmenite. Garnets enclosed by andalusite crystals were observed, however garnet was not consumed during andalusite growth (Figure A2.-5). Biotite porphyroblasts are 1.0-2.0 mm in size and sometimes
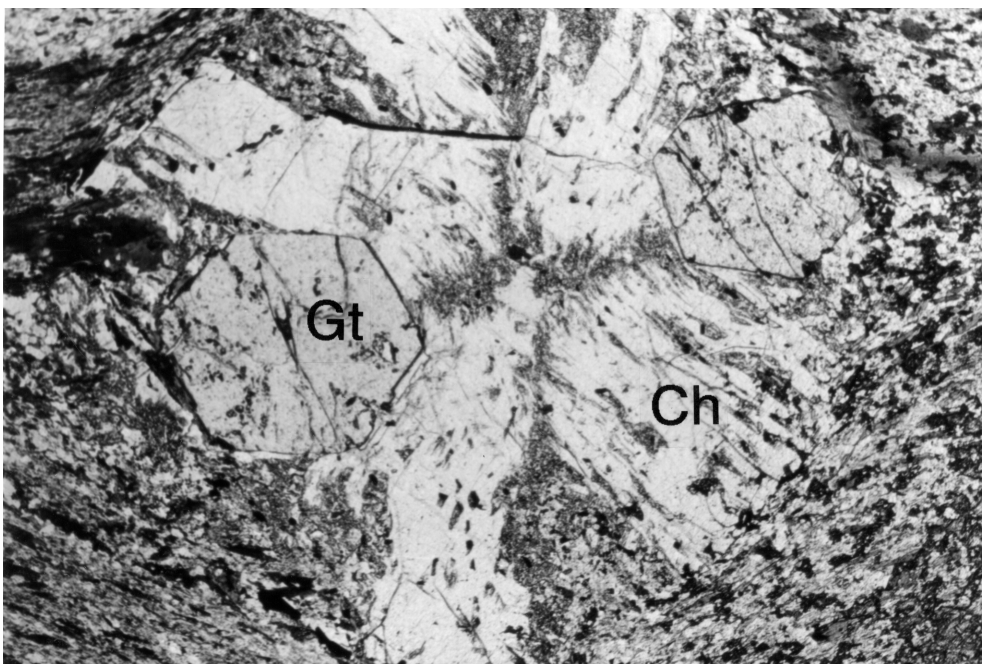
Figure A.2-5: Garnet enclosed by chiastolite in sample Kid 18 from the Malhaq Fm.. The garnet rims are well preserved, indicating no reaction of garnet during chiastolite growth. Magnification 30x.

overgrow the foliation. Hornblende is also present as porphyroblasts and up to 1 mm in size. They are found in the form of flakes and aggregates. Chlorite is only present in minor quantities. Ilmenite and magnetite are accessory minerals.

The *Heib Fm.* consists of upper-greenschist to lower-amphibolite-grade biotite-muscovite schists. These contain fine-grained feldspar, quartz, biotite, muscovite and chlorite. Porphyroblasts consist of cordierite, biotite and garnet. Biotite, muscovite and chlorite define the foliation.

The *Tarr Fm.* consists of low-grade schists, mudstones, sandstones, conglomerates and andesitic flows. The Tarr Fm. comprises the Beda Turbidites that formerly had been included in the Heib Fm (Blasband et al., 1997). The turbidites show sedimentary structures, such as fining-up sequences and low angle structures. The conglomerates contain granitic, andesitic and pelitic pebbles. Biotite schists form shear zones, 50-100m thick, that cross cut the Tarr Fm. These shear zones are formed in the highly schistose parts of the Tarr Fm. and are considered to be splays off the deeper shear (Blasband et al., 2000). The Tarr Fm. overlies the Heib Fm. On the basis of major and trace element studies Furnes et al. (1985) concluded that the protoliths of the Malhaq Fm., Heib Fm., Umm Zariq Fm. and Tarr Fm. exhibit trace element abundance's and ratios that characterize subduction-related rocks.

The *Quneia Fm.* is plutonic in origin and consists of foliated and lineated diorites and tonalites. Similar intrusives in the Nuweiba area (100 km north of the Wadi Kid Complex) were interpreted as subduction-related I-type intrusives (Ahmed et al., 1993).

The *Sharira Diorite* is an undeformed hornblende-diorite in the northern part of the Wadi Kid area and was dated at 570±4 Ma (Moghazi et al, 1998).

All formations, except the Tarr Fm., are intruded by undeformed to slightly deformed biotite bearing alkaline granites, which were interpreted as A-type granites by Ahmed et al. (1993). Trace-element studies on similar granites in the Timna Area show that these granites are related to crustal thinning in an extensional regime (Beyth et al., 1994). Mafic and felsic composite dykes crosscut the upper and lower crustal rocks in NE-SW direction. Undeformed ignimbrites and rhyolites overlie the Tarr Fm.

A.2.3 Structures

An extensive structural study of the Wadi Kid area was conducted by Blasband et al. (1997, 2000). They recognized two deformation phases in the Late Proterozoic history of the Wadi Kid area. The older phase, hereby referred to as D_1 produced a steep regional foliation, axial planar to F_1 folds with WSW-ENE fold-axes. This phase is only observed in upper-crustal rocks of the Tarr Fm. Deformation took place at greenschist facies conditions. This D_1 phase is thought to have been related to arc-accretion and was interpreted to have taken place at 720-650 Ma (Blasband et al., 2000).

The younger deformation phase, D_2, produced structures in the lower- and upper-crustal rocks (Blasband et al., 1997, 2000). The structures include an S_2-foliation, a NW-SE trending L_2 lineation formed by hornblende, andalusite, mica pods and stretched feldspars (Blasband et al., 1997). Dikes intruded in a NE-SW direction, perpendicular to the stretching lineation, and indicate NW-SE extension during D_2. Shear sense indicators, specifically deformed xenoliths

and conglomerates, extensional crenulation cleavages, rotated porphyroclasts with pressure shadows and S-C fabrics, indicate that the schists were formed as normal shear zones in an extensional environment (Blasband et al., 1997, 2000). The main sense of movement was to the NW but local reversals to the SE were recorded (Blasband et al., 1997). The reversal was related to the doming of the lower crust, which is caused by isostatic rebound of the crust and intrusion of A-type granites (Blasband et al., 1997, 2000).

A.2.4 Petrology

Seven samples from the Malhaq Fm. and Umm Zariq Fm. were selected for geothermobarometry. The petrology of these samples will be described below. The objective of this paragraph is to unravel the P-T conditions of the mineral assemblages in the samples and to compare it with a P-T diagram showing the univariant curves for the reactions that control the appearance and breakdown of the phases present. The order of mineral growth and mineral reactions seen in the thin sections define a PTt path, where as geothermobarometry studies will define a single point in PTt-space.

Sample Kid 18 is a garnet-andalusite-biotite schist from the Malhaq Fm. In sample Kid 18 garnet is enclosed by andalusite (Figures A.2-4 and A.2-5), suggesting garnet grew before andalusite through the reaction

- chlorite + muscovite = garnet + biotite + quartz + H_2O.

Andalusite grew through the reaction, thereby not consuming garnet as garnet remained stable during andalusite growth,

- pyrophyllite = andalusite + quartz + H_2O.

In sample Kid 18 we also observed breakdown of andalusite overgrown by muscovite through the reaction

- andalusite + K-feldspar + H_2O = muscovite.

Sample B 63 is a garnet-biotite schist from the Malhaq Fm. hereby we assume that as a resultant of metamorphism during D_1 sample B 63 is a chlorite-muscovite schist comparable with the Beda turbidites and during D_2 garnet and biotite were formed through the reaction

- chlorite + muscovite = garnet + biotite + quartz + H_2O.

The order of mineral growth in sample Kid 6, Umm Zariq Fm., is probably staurolite, followed by garnet and andalusite. Staurolite (Figure A.2-2) can exist in low and medium pressure rocks and can be formed by the following reactions (Yardley, 1989)

- chloritoid + quartz = staurolite + garnet + H_2O or
- garnet + muscovite + chlorite = staurolite + biotite + quartz + H_2O or
- chlorite + muscovite = staurolite + biotite + quartz + H_2O.

In the samples no relics of chloritoid is found and garnet is formed after staurolite, thereby leaving the third reaction as most likely.

Garnet was formed not at the expense of staurolite through the reaction

- chlorite + muscovite = garnet + biotite + quartz + H_2O,

thereby forming the stable assemblage staurolite-garnet-biotite.

Transformation of staurolite into andalusite was observed in sample Kid 6 through the reaction

- staurolite + muscovite + quartz = andalusite + biotite + H_2O.

Andalusite breakdown observed in sample Kid 6 to form muscovite through the reaction (Figure A.2-3)

- andalusite + K-feldspar + H_2O = muscovite.

During the last phase of metamorphism H_2O is needed for retrograde reactions. During this phase the post-tectonic granites were probably the main source of H_2O.

Sample Kid 2 is a garnet-biotite schist were garnet and biotite formed through the reaction like sample B 63

- chlorite + muscovite = garnet + biotite + quartz + H_2O.

A.2.5 Mineral composition

A.2.5.1 Methods

The purpose of obtaining exact mineral compositions is to use the data for geotermobarometry and to derive exact pressure and temperature conditions for the samples. Geothermobarometry is the name given to the application whereby the pressure and temperature dependence of the equilibrium constant is used to infer metamorphic pressures and temperatures. The most common geothermometer in pelitic schists is based on the cation exchange reaction of Fe en Mg between garnet and biotite.

Mineral compositions were determined by analyzing carbon-coated, polished thin sections on the JEOL JXA-8600 microprobe at Utrecht University. Operating conditions were 15 kV accelerating potential and 10 nA beam current. A focused beam diameter of <1 µm was used for all minerals. Standard ten-element analyses were performed on all minerals. SiO_2, Al_2O_3, FeO, CaO, MgO and K_2O were analyzed on the energy dispersive X-ray spectrometer and TiO_2, Na_2O, Cr_2O_3 and MnO were analyzed on the wavelength dispersive X-ray spectrometer. Analyses on garnets were core-rim in small steps. Core and rim analyses were made on biotite porphyroblasts, andalusites, amphibole porphyroblasts, K-feldspars, plagioclase and staurolite. Measurements on muscovite, chlorite, biotite and ilmenite were spot analyses.

Biotite grains near garnet, but not in physical contact with garnet, were used for geothermometry, because these biotites are considered to reflect the composition at the peak temperature. It was assumed that the composition of biotite is not influenced by post-metamorphic diffusion.

Conditions of metamorphism reflected by the pelitic schists were estimated by using biotite-garnet thermometry using the calibration of Kleemann and Reinhardt (1994). In the Kleemann and Reinhardt (1994) model, Mg-Fe mixing is assumed to be ideal, whereas the activity model is non-ideal for Mg, Fe-Al and Mg, Fe-Ti mixing. The titanium mixing parameters used in this study were taken from Sengupta et al. (1990). According to Kleemann and Reinhardt (1994) the influence of Ti on garnet-biotite thermometry is small compared to the effect of ^{VI}Al and is considered to be negligible. The garnet activity model was taken from Berman (1990). Pressures were estimated using the plagioclase-biotite-muscovite-garnet geobarometer of Powell and Holland (1988), originally calibrated by Ghent and Stout (1981). This barometer is especially suitable for rocks in which aluminosilicate polymorphs are absent.

The best estimate for peak temperatures during M_2 comes from thermobarometry

combining matrix phases with the low Fe/(Fe+Mg) region of the garnet (the "well") just inside the rim. (Spear, 1991). This low X_{Fe} region represents the minimum estimate of peak temperature (Spear, 1991).

Geothermobarometry on mafic schists is based on the chemical interaction between plagioclase and hornblende. Several geothermometers are available and geobarometers are rare. In this study the hornblende-plagioclase geothermometer of Holland and Blundy (1994) was used. The Holland and Blundy (1994) thermometer is based on an ideal mixing-on-sites model for amphibole and plagioclase non-ideality is modeled on the basis of Darken's quadratic formalism (Holland and Powell, 1992). A problem associated with the use of amphiboles and plagioclase in geothermobarometry is that both solid solutions show miscibility gaps. Furthermore, the disadvantage of this thermometer is that it uses fixed pressures. Results obtained by the Holland and Blundy (1994) calibration were calculated using HBL-PLAG, a computer program that requires raw microprobe data and the activity of albite. It computes temperatures for different pressures.

A.2.5.2 Chemical compositions

A.2.5.2.1 Pelitic schists of the Malhaq Formation

The samples Kid 18 and B 63 represent the metapelites of the Malhaq Fm. Kid 18 is a garnet-andalusite-biotite schist and sample B 63 is a garnet-biotite schist. Tables A.2-1 and A.2-2 summarize the chemical compositions of the minerals from this pelitic schist. Sample locations are shown in Figure A.2-1. In the garnets the mole fractions of almandine ranges between 0.67 and 0.80 (see Figures A.2-6 and A.2-7). Pyrope, spessartine and grossular contents vary between 0.03 and 0.17. Most garnets show an increase in almandine and pyrope from core to rim, whereas spessartine and grossular decrease (see Figures A.2-6 and A.2-7). Biotite composition differs between sample Kid 18 and sample B 63. X_{Fe} varies between 0.65 and 0.71 in sample Kid 18 and between 0.52 and 0.56 in sample B 63. The potassium content of muscovite varies between 0.81-0.92 (Kid 18) and 0.95-0.98 (sample B 63). Plagioclase feldspars in sample Kid 18 are rich in albite (X_{Ab}= 0.63-0.88) with only minor amounts of orthoclase (X_{Or}= 0.0-0.08).

A.2.5.2.2 Pelitic schists of the Umm Zariq Formation

Tables A.2-3 and A.2-4 summarize representative microprobe analyses for sample Kid 6, a garnet-andalusite-staurolite-biotite schist, and sample Kid 2, a garnet-biotite schist. The sample locations are shown in Figure A.2-1. The mole fraction of almandine in garnets from the Umm Zariq Fm. ranges between 0.61-0.80 (Figures A.2-8 and A.2-9). The mole fractions of pyrope, spessartine and grossular are lower and vary between 0.04-0.16 (Figures A.2-8 and A.2-9). Almandine increases from core to rim in all samples, pyrope shows a flat profile or a slight decrease, spessartine decreases from core to rim in both samples (Figures A.2-8 and A.2-9). X_{Fe} in biotite varies between 0.58-0.66 in sample Kid 6 and between 0.48-0.52 in sample Kid 2. X_{Mg} in biotite varies between 0.21 and 0.39. Muscovite in sample Kid 6 has potassium content

Table A.2-1 Representative results of electron microprobe analyses of garnet, biotite, muscovite and plagioclase in sample Kid 18. For location see Figure A.2-6. Oxygen basis of the analysis: Pl 8; Grt 24; Bt, Ms 22. $X_{Fe} = Fe/(Fe+Mg)$; $X_{Alm} = Fe/(Fe+Mg+Mn+Ca)$; $X_{Sps} = Mn/(Fe+Mg+Mn+Ca)$; $X_{Prp} = Mg/(Fe+Mg+Mn+Ca)$; $X_{Grs} = Ca/(Fe+Mg+Mn+Ca)$; $X_{Ab} = Na/(Na+K+Ca)$.

Kid 18

	Gt 1 core	Gt 1 rim	Gt 4 core	Gt 4 rim	90 Bt matrix	126 Bt matrix	9 Ms matrix	78 Ms matrix	13 Pl matrix	1 Pl matrix
SiO_2	36.26	37.82	36.43	37.05	33.07	32.13	47.99	48.01	61.04	61.41
TiO_2	0.03	0.07	0.98	-	2.37	2.07	0.28	0.47	-	-
Al_2O_3	20.71	20.82	20.58	20.63	18.89	18.69	38.05	37.68	25.09	24.53
Cr_2O_3	-	-	-	-	-	-	0.01	0.04	-	-
FeO	33.28	36.27	32.06	35.76	24.71	26.80	1.07	1.22	-	0.32
MnO	6.77	3.65	6.83	3.85	0.15	0.17	0.04	-	-	-
CaO	2.28	2.38	2.20	2.27	-	0.17	-	-	6.56	5.88
MgO	1.23	1.66	0.91	1.81	5.94	6.96	0.13	0.23	-	-
K_2O	-	-	-	-	8.82	6.77	8.84	8.49	0.14	-
Na_2O	0.12	-	0.09	-	0.08	0.11	0.65	0.54	8.10	8.69
Total	100.68	102.67	100.08	101.37	94.03	93.87	97.06	96.68	100.93	100.83
Si	5.914	6.012	5.944	5.972	5.254	5.124	6.170	6.188	2.691	2.712
Ti	0.003	0.007	0.121	-	0.283	0.239	0.027	0.045	-	-
Al	3.982	3.901	3.956	3.921	3.674	3.511	5.769	5.725	1.304	1.277
Cr	-	-	-	-	0.001	-	0.001	0.003	-	-
Fe	4.541	4.820	4.373	4.821	3.283	3.575	0.116	0.132	-	0.012
Mn	0.934	0.492	0.944	0.525	0.020	0.023	0.003	-	-	-
Ca	0.399	0.406	0.383	0.393	-	0.029	-	-	0.310	0.278
Mg	0.300	0.391	0.221	0.436	1.404	1.655	0.025	0.046	-	-
K	-	-	-	-	1.787	1.377	1.451	1.397	0.008	-
Na	0.040	-	0.031	-	0.026	0.034	0.162	0.133	0.693	0.744
Total	16.113	16.029	15.973	16.068	15.732	15.568	13.724	13.669	5.006	5.023
X_{Fe}	0.960	0.925	0.952	0.917	0.701	0.684	-	-	-	-
X_{Alm}	0.747	0.789	0.739	0.781	-	-	-	-	-	-
X_{Sps}	0.153	0.081	0.159	0.085	-	-	-	-	-	-
X_{Prp}	0.031	0.064	0.037	0.071	-	-	-	-	-	-
X_{Grs}	0.070	0.066	0.065	0.064	-	-	-	-	-	-
X_{Ab}	-	-	-	-	-	-	-	-	0.685	0.728

Table A.2-2: Representative results of electron microprobe analyses of hornblende, plagioclase and chlorite in sample B 64. For location see Figure A.2-6. Oxygen basis of the analysis: Hbl 23; Pl 8; Chl 28. X_{Fe} = Fe/

	Hbl 2.1	Hbl 2.3	Hbl 2	Hbl 4	Hbl 5	Hbl 12	Pl 1	Pl 5	Pl 8	Chl 1
	blast	blast	matrix	matrix	matrix	matrix	matrix	matrix	matrix	matrix
SiO_2	44.04	44.37	48.07	45.04	44.91	44.12	46.36	47.51	67.49	25.64
TiO_2	0.72	0.65	0.53	0.58	0.59	0.66	-	0.06	0.01	0.08
Al_2O_3	12.5	12.75	8.58	11.78	12.40	13.34	35.23	34.40	20.74	21.46
Cr_2O_3	0.03	-	0.04	-	-	0.29	-	-	0.01	0.03
FeO	20.19	19.55	18.95	19.75	19.98	19.59	0.23	0.27	0.36	28.16
MnO	0.45	0.43	0.51	0.50	0.49	0.45	0.02	-	-	0.34
CaO	12.17	11.73	11.59	11.65	11.89	11.76	18.75	17.62	1.49	-
MgO	8.06	8.53	10.26	8.72	8.06	8.03	-	-	-	15.04
K_2O	0.61	0.48	0.33	0.40	0.44	0.61	-	-	1.70	-
Na_2O	0.91	1.08	0.78	0.94	1.05	1.09	1.25	1.81	8.64	0.03
Total	99.69	99.57	99.64	99.34	99.81	99.95	101.83	101.67	100.43	90.79
Si	6.539	6.558	7.037	6.668	6.629	6.507	2.101	2.150	2.950	5.293
Ti	0.081	0.072	0.059	0.064	0.066	0.073	-	0.002	0.001	0.012
Al	2.187	2.221	1.480	2.055	2.157	2.319	1.882	1.835	1.068	5.220
Cr	0.003	-	0.005	-	-	0.033	-	-	-	0.006
Fe	2.507	2.417	2.320	2.445	2.466	2.416	0.009	0.010	0.013	4.862
Mn	0.057	0.054	0.063	0.062	0.062	0.056	0.001	-	-	0.058
Ca	1.937	1.858	1.818	1.848	1.880	1.858	0.910	0.855	0.070	-
Mg	1.784	1.880	2.238	1.924	1.774	1.766	-	-	-	4.627
K	0.116	0.090	0.062	0.076	0.083	0.114	-	-	0.095	-
Na	0.262	0.308	0.221	0.269	0.301	0.313	0.110	0.159	0.732	0.012
Total	15.473	15.458	15.303	15.411	15.418	15.455	5.013	5.011	4.929	20.090
X_{Fe}	0.584	0.562	0.509	0.560	0.582	0.578				0.512
X_{Ab}							0.108	0.157	0.816	

Table A.2-3: Representative results of electron microprobe analyses of garnet, biotite, muscovite, staurolite and plagioclase in sample Kid 6. For location see Figure A.2-6. Oxygen basis of the analysis: Pl 8; Grt 24; Bt, Ms 22; St 32. $X_{Fe} = Fe/(Fe+Mg)$; $X_{Alm} = Fe/(Fe+Mg+Mn+Ca)$; $X_{Sps} = Mn/(Fe+Mg+Mn+Ca)$; $X_{Prp} = Mg/(Fe+Mg+Mn+Ca)$; $X_{Grs} = Ca/(Fe+Mg+Mn+Ca)$; $X_{Ab} = Na/(Na+K+Ca)$.

Kid 6

|	Gt 3 core	Gt 3 rim	Gt 6 core	Gt 6 rim	Bt 1 matrix	Bt 8 matrix	Ms 1 matrix	St 1	Pl 4 matrix	Pl 7 matrix
SiO_2	37.58	37.31	36.52	37.55	35.36	34.68	46.59	27.53	60.87	59.90
TiO_2	-	0.01	-	-	0.98	2.13	0.44	0.52	-	0.05
Al_2O_3	20.93	21.38	20.88	20.84	21.08	20.67	37.51	54.06	25.38	25.31
Cr_2O_3	0.04	0.01	0.01	-	-	-	0.04	0.04	0.05	-
FeO	33.27	35.22	33.13	34.99	20.74	21.91	1.03	13.77	-	0.31
MnO	6.27	4.27	6.25	3.89	0.14	0.1	-	0.22	-	-
CaO	1.56	1.88	1.94	1.90	0.13	-	-	-	6.77	6.44
MgO	1.32	1.77	1.66	1.66	8.19	7.22	-	1.09	-	-
K_2O	0.14	0.11	-	0.10	9.42	9.93	8.87	-	0.18	0.48
Na_2O	0.03	0.03	0.07	0.11	0.22	0.14	0.64	-	7.75	7.68
Total	101.15	102.00	100.46	101.04	96.26	96.79	95.12	97.23	100.99	100.16
Si	6.049	5.959	5.938	6.039	5.347	5.271	6.125	5.347	2.682	2.669
Ti	-	0.001	-	-	0.112	0.244	0.043	0.075	-	0.002
Al	3.970	4.025	4.003	3.953	3.757	3.702	5.812	12.372	1.318	1.329
Cr	0.005	0.001	0.002	-	-	-	0.004	0.007	0.002	-
Fe	4.479	4.704	4.505	4.708	2.623	2.786	0.114	2.235	-	0.012
Mn	0.855	0.577	0.861	0.530	0.017	0.014	-	0.036	-	-
Ca	0.269	0.322	0.338	0.328	0.021	-	-	-	0.220	0.307
Mg	0.317	0.421	0.404	0.399	1.847	1.636	-	0.317	-	-
K	0.029	0.023	-	0.020	1.818	1.926	1.488	-	0.010	0.027
Na	0.010	0.009	0.021	0.039	0.066	0.041	0.164	-	0.663	0.660
Total	15.983	16.042	16.072	16.016	15.608	15.620	13.750	20.389	4.865	5.006
X_{Fe}	0.934	0.918	0.918	0.922	0.587	0.630				
X_{Alm}	0.757	0.781	0.738	0.789						
X_{Sps}	0.144	0.096	0.066	0.067						
X_{Prp}	0.054	0.070	0.055	0.055						
X_{Grs}	0.045	0.053	0.141	0.089						
X_{Ab}								0.876	0.742	0.665

Table A.2-4: Representative results of electron microprobe analyses of garnet, biotite, chlorite and plagioclase in sample Kid 2. For location see Figure A.2-6. Oxygen basis of the analysis: Pl 8; Grt 24; Bt, Ms 22; Chl 28. X_{Fe} = Fe/(Fe+Mg); X_{Alm} = Fe/(Fe+Mg+Mn+Ca); X_{Sps} = Mn/(Fe+Mg+Mn+Ca); X_{Prp} = Mg/(Fe+Mg+Mn+Ca); X_{Grs} = Ca/(Fe+Mg+Mn+Ca); X_{Ab} = Na/(Na+K+Ca).

|	Kid 2							
	Grt 1	Grt 1	Grt 2	Grt 2	Bt 52	Chl 44	Pl 50	Pl 51
	core	rim	core	rim	matrix	matrix	matrix	matrix
SiO_2	37.01	36.41	37.85	37.82	36.32	26.31	57.55	56.95
TiO_2	0.07	0.05	0.10	0.10	1.99	0.15	0.02	-
Al_2O_3	20.97	21.05	21.29	21.20	18.09	21.79	26.60	27.78
Cr_2O_3	0.06	0.07	-	-	-	-	-	-
FeO	29.38	37.42	29.63	32.02	20.42	25.55	0.06	-
MnO	5.69	3.81	5.32	3.83	0.08	0.19	-	-
CaO	4.34	2.88	4.53	2.70	0.03	0.06	8.69	9.60
MgO	1.67	2.24	1.72	2.47	10.48	14.87	0.02	-
K_2O	-	-	-	-	8.98	0.22	0.06	0.05
Na_2O	-	0.01	0.01	-	0.04	0.01	6.25	6.30
Total	99.19	97.94	100.45	100.57	96.42	89.15	99.25	100.68
Si	6.009	5.981	6.046	6.031	5.466	5.445	2.592	2.539
Ti	0.010	0.006	0.012	0.011	0.226	0.025	0.001	-
Al	3.977	4.745	4.011	4.034	3.208	5.315	1.412	1.459
Cr	0.008	0.009	-	-	-	-	-	-
Fe	3.846	4.315	3.958	4.409	2.569	4.423	0.002	-
Mn	0.745	0.530	0.720	0.431	0.011	0.034	-	-
Ca	0.849	0.507	0.776	0.385	0.005	0.014	0.420	0.458
Mg	0.399	0.549	0.410	0.640	2.351	4.589	0.001	-
K	-	-	-	-	1.732	0.057	0.004	0.003
Na	-	0.003	0.006	-	0.013	0.004	0.546	0.544
Total	15.974	16.645	15.939	15.941	15.572	19.906	4.798	5.003
X_{Fe}	0.908	0.887	0.906	0.873	0.522	0.491		
X_{Alm}	0.673	0.731	0.675	0.752				
X_{Sps}	0.132	0.090	0.123	0.074				
X_{Prp}	0.068	0.093	0.070	0.109				
X_{Grs}	0.127	0.086	0.132	0.066				
X_{Ab}							0.563	0.541
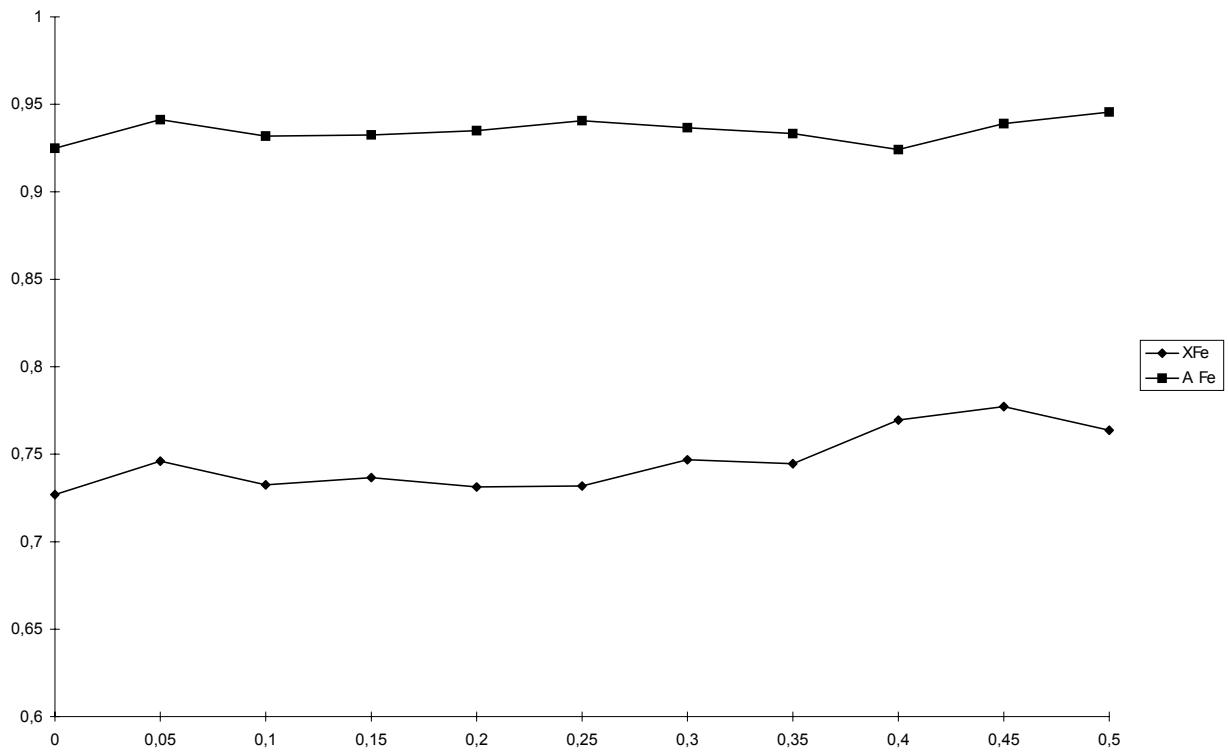
a
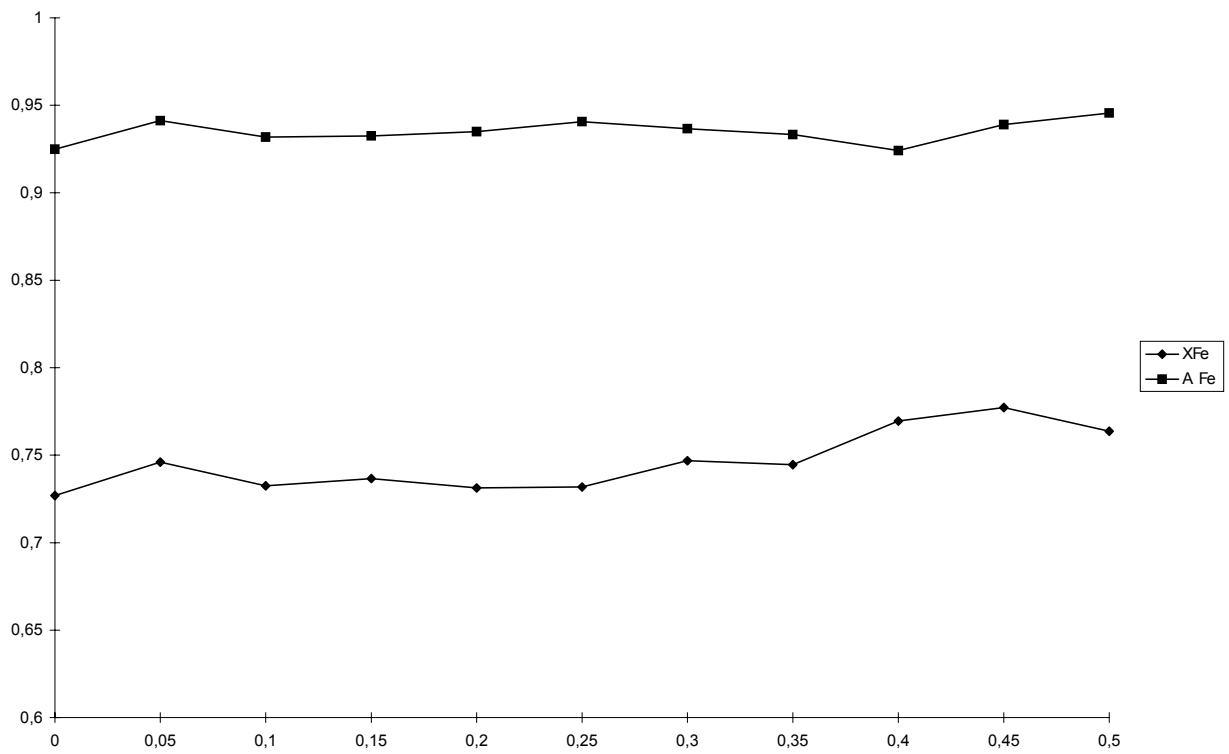
b

Figure A.2-6 a) shows trends for A_{Fe} (top) and X_{Fe}, garnet 6, Kid 18; b) Shows trends for B_{Mn}, X_{Mn} (top two lines), X_{Mg} (at 0,06) and X_{Ca} for garnet 6, Kid 18.
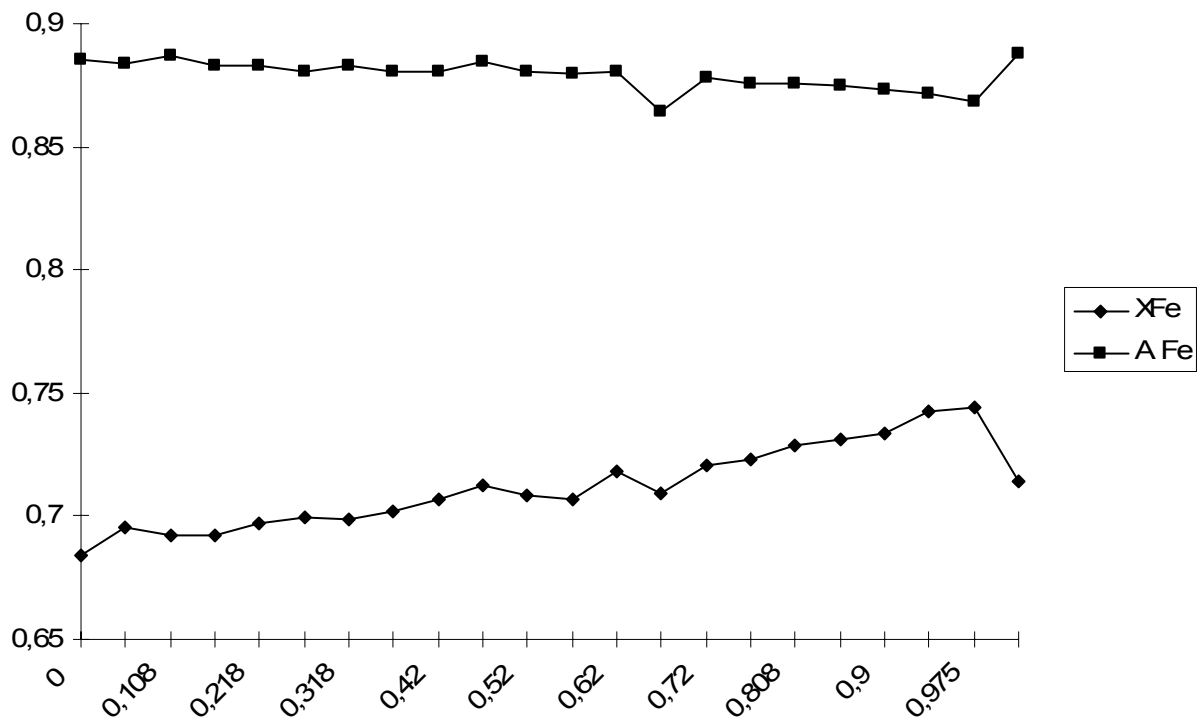
a
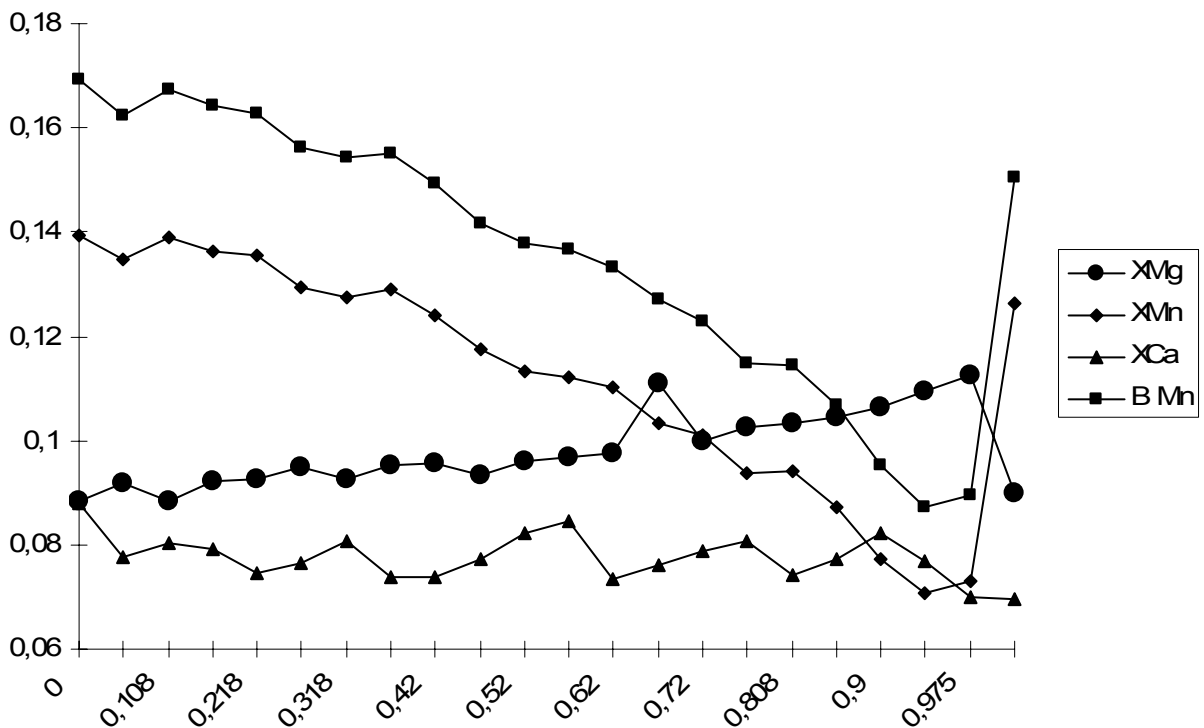
b

Figure A.2-7 a) shows trends of AFe (top) and XFe, garnet 1, sample B63; b) shows trends for BMn and XMn (top two), XMg (third line) and XCa (bottom line), garnet 1, sample B 63.

of 0.90. Plagioclase in sample Kid 6 has an anorthite content between 0.20-0.38. K-feldspar is also observed. Plagioclase is commonly found in Kid 2. The mole fraction of magnesium in staurolite in Kid 6 varies between 0.12 and 0.15. Ilmenite is present in both samples with mole fractions of manganese varying between 0.02 and 0.18.

A.2.5.2.3 Metavolcanics of the Malhaq Formation

Tables A.2-5 to A.2-7 summarize the composition of minerals from samples of metavolcanic rocks of the Malhaq Fm. Sample locations are shown in Figure A.2-1. Sample B 61 is a biotite-amphibole schist and samples B 64 and WJ 64 are amphibole schists. All amphiboles are calcic in composition according to the classification scheme of Leake (1978). The X_{Mg} is between 0.43 and 0.82. No zoning is observed. Feldspar composition has grain to grain variations from albite to orthoclase in the different samples. The mole fraction of iron in biotite varies around 0.43 and the mole fraction of magnesium is around 0.46. Chlorite is only present in minor amounts and has an X_{Fe} between 0.39 and 0.51.

A.2.5.3 PT conditions

Tables A.2-8 to A.2-10 summarize the calculated temperatures and pressures for the different samples. The pelitic schists of the Central Wadi Kid area recorded garnet rim temperatures of 533 to 567°C (Table A.2-8). Garnet core temperatures are between 488 and 536°C (Table A.2-8). Pressures in the Wadi Kid area are consistent and are in the range 3-4.5 kbar (Table A.2-8).

Metamorphic conditions recorded by the metapelites in the Wadi Lig (sample B 63), in the northern part of the Wadi Kid area (Figure A.2-1), recorded garnet rim temperatures of 604-620°C and a pressure of 4.19 kbar (Table A.2-9), indicating upper-amphibolite facies conditions. Garnet core temperatures are slightly lower between 587 and 590°C. Metamorphic conditions estimated from hornblende-plagioclase thermometry were calculated for all measured amphiboles in the mafic schists (samples B61, B63 and WJ 61). Average temperatures for the amphiboles in the mafic schists range from 565 to 678°C with a pressure of 4 kbar (Table A.2-10).

In order to derive a PTt-path it is useful to compare the petrology and mineral assemblages in the pelitic schists with a petrogenetic grid. In this paper the KFMASH grid of Spear and Cheney (1989, Figure A.2-10) is used. Garnet-andalusite-biotite assemblages are stable between 550-600 °C and below the 3 kbar. Staurolite breakdown occurs between 500-600 °C and 1-3 kbar. Garnet-biotite assemblages are stable above 475 °C and less than 3 kbar up into the sillimanite stability field. The staurolite-andalusite stability field starts at approximately 475 °C. Mineral assemblages in the pelitic rocks indicate greenschist to amphibolite metamorphism. The metamorphic facies classification for mafic rocks is due to less sensitivity of the minerals to changes in pressure and temperature not so clear as for pelitic rocks.

Table A.2-5: Representative results of electron microprobe analyses of hornblende, plagioclase, chlorite and biotite in sample B 61. For location see Figure A.2-6. Oxygen basis of the analysis: Hbl, Bt 23; Pl 8; Chl 28. X_{Fe} = Fe/(Fe+Mg); X_{Ab} = Na/(Na+K+Ca).

|					B 61				
	Hbl 2	Hbl 21	Hbl 24	Hbl 32	Pl 11	Pl 25	Pl 36	Chl 22	Bt 12
	matrix	matrix	matrix	matrix	matrix	matrix	matrix	matrix	matrix
SiO_2	46.06	46.02	46.34	46.30	60.01	68.91	59.00	27.26	36.41
TiO_2	0.35	0.37	0.35	0.33	-	0.03	-	0.02	2.20
Al_2O_3	9.94	10.15	10.56	10.28	25.55	21.09	26.68	20.05	15.97
Cr_2O_3	-	-	-	-	-	0.01	-	-	-
FeO	15.90	15.22	14.29	15.22	0.06	0.06	0.12	23.05	17.42
MnO	0.41	0.43	0.40	0.35	-	-	-	0.27	0.17
CaO	11.98	11.80	11.74	11.74	6.98	2.01	7.67	0.13	0.08
MgO	12.35	12.77	13.13	12.30	-	-	0.02	18.09	13.15
K_2O	0.33	0.33	0.39	0.27	0.14	0.06	0.13	0.02	8.90
Na_2O	1.08	1.13	1.15	1.09	7.41	7.70	7.29	0.01	0.09
Total	98.40	98.22	98.35	97.88	100.15	99.87	100.91	88.90	94.39
Si	6.774	6.758	6.759	6.808	2.667	2.982	2.613	5.586	5.794
Ti	0.039	0.041	0.039	0.037	-	0.001	-	0.001	0.265
Al	1.723	1.756	1.815	1.780	1.338	1.075	1.392	4.843	2.995
Cr	-	-	-	-	-	0.0004	-	-	-
Fe	1.955	1.870	1.744	1.871	0.002	0.003	0.004	3.952	2.317
Mn	0.052	0.054	0.049	0.044	-	-	-	0.047	0.023
Ca	1.888	1.855	1.835	1.849	0.333	0.093	0.364	0.029	0.015
Mg	2.708	2.974	2.855	2.695	-	-	0.001	5.527	3.118
K	0.062	0.061	0.071	0.049	0.008	0.004	0.072	0.005	1.806
Na	0.308	0.322	0.326	0.309	0.639	0.646	0.627	0.007	0.029
Total	15.509	15.511	15.493	15.442	4.987	4.804	5.0732	19.637	16.362
X_{Fe}	0.419	0.386	0.379	0.410				0.417	
X_{Ab}					0.652	0.869	0.590		

Table A.2-6: Representative results of electron microprobe analyses in sample B 63. For location see Figure A.2-6. Oxygen basis of the analysis: Pl 8; Grt 24; Bt, Ms 22. $X_{Fe} = Fe/(Fe+Mg)$; $X_{Alm} = Fe/(Fe+Mg+Mn+Ca)$; $X_{Sps} = Mn/(Fe+Mg+Mn+Ca)$; $X_{Prp} = Mg/(Fe+Mg+Mn+Ca)$; $X_{Grs} = Ca/(Fe+Mg+Mn+Ca)$; $X_{Ab} = Na/(Na+K+Ca)$.

|	Gt 1 core	Gt 1 rim	Gt 2 core	Gt 2 rim	Bt 150 matrix	Bt 158 matrix	Ms 154 matrix	Pl 152 matrix	Pl 135 matrix
SiO_2	37.52	35.21	37.40	34.40	34.55	34.42	47.66	56.44	56.22
TiO_2	0.07	0.02	0.03	0.02	1.13	1.25	1.07	-	-
Al_2O_3	21.07	20.54	21.14	21.96	20.27	20.22	37.51	28.38	28.17
Cr_2O_3	-	-	-	0.03	-	0.06	-	-	-
FeO	29.53	31.63	29.02	28.61	21.29	21.10	1.57	-	0.05
MnO	5.94	3.07	6.79	4.47	0.19	0.15	-	0.03	0.03
CaO	2.95	2.32	2.42	2.64	0.04	0.17	0.01	9.57	9.57
MgO	2.14	2.69	2.12	2.11	8.16	9.80	0.81	-	-
K_2O	-	-	-	0.10	9.93	7.30	6.73	0.10	0.10
Na_2O	0.01	0.01	0.03	0.08	0.09	0.08	0.19	6.13	5.76
Total	99.23	95.49	98.95	94.42	95.65	94.55	95.55	100.65	99.90
Si	6.064	5.938	6.062	5.834	5.307	5.265	6.159	2.517	2.524
Ti	0.008	0.002	0.004	0.003	0.131	0.145	0.104	-	-
Al	4.013	4.081	4.041	4.388	3.671	3.644	5.713	1.493	1.491
Cr	0.001	-	-	0.003	-	0.007	-	-	-
Fe	3.992	4.463	3.934	4.059	2.734	2.699	0.170	-	0.002
Mn	0.814	0.439	0.933	0.642	0.025	0.019	-	0.001	0.001
Ca	0.512	0.420	0.421	0.481	0.006	0.027	0.002	0.457	0.460
Mg	0.515	0.674	0.514	0.534	1.866	2.235	0.155	-	-
K	-	0.001	-	0.020	1.943	1.425	1.110	0.005	0.006
Na	0.006	0.006	0.089	0.026	0.027	0.022	0.048	0.531	0.501
Total	15.925	16.478	15.998	15.990	15.710	15.488	13.461	5.004	4.985
X_{Fe}	0.886	0.869	0.884	0.884	0.594	0.547			
X_{Alm}	0.684	0.744	0.678	0.710					
X_{Sps}	0.140	0.073	0.161	0.112					
X_{Prp}	0.088	0.112	0.089	0.093					
X_{Grs}	0.088	0.070	0.073	0.084					
X_{Ab}								0.534	0.518

Table A.2-7: Representative results of electron microprobe analyses in sample WJ 61. For location see Figure A.2-6. Oxygen basis of the analysis: Hbl 23; Pl 8; Chl 28. X_{Fe} = Fe/(Fe+Mg); X_{Ab} = Na/(Na+K+Ca).

|											WJ 61
	Hbl 72	Hbl 77	Hbl 90	Hbl 94	Hbl 102	Hbl 103	Pl 71	Pl 86	Pl 96	Pl 100	Chl 97
	matrix	matrix	matrix	matrix	matrix	matrix	matrix	matrix	matrix	matrix	matrix
SiO_2	45.10	45.55	45.16	43.96	46.15	48.50	63.37	64.52	63.13	64.52	26.68
TiO_2	0.53	0.52	0.53	0.60	0.40	0.42	-	-	-	-	0.15
Al_2O_3	10.58	10.17	10.49	11.05	9.60	7.12	23.49	23.71	23.81	21.33	19.61
Cr_2O_3	0.01	0.07	0.34	0.04	-	0.03	0.01	-	0.03	-	0.06
FeO	19.63	19.22	19.17	19.85	18.78	18.26	0.17	0.06	0.10	0.08	28.02
MnO	0.37	0.36	0.36	0.30	0.32	0.34	-	0.01	-	0.01	0.19
CaO	10.89	10.82	10.80	11.00	11.12	10.94	4.63	4.58	4.32	0.32	0.15
MgO	9.85	10.10	9.95	9.35	10.74	11.66	-	-	-	0.03	12.62
K_2O	0.34	0.33	0.33	0.35	0.28	0.22	0.06	0.11	0.06	11.43	0.04
Na_2O	1.52	1.50	1.52	1.60	1.29	0.97	6.79	9.23	9.44	2.20	-
Total	98.82	98.64	98.65	98.10	98.68	98.46	98.52	102.22	100.89	99.92	87.52
Si	6.713	6.777	6.724	6.619	6.839	7.152	2.816	2.791	2.770	2.922	5.706
Ti	0.061	0.058	0.059	0.067	0.046	0.047	-	-	-	-	0.025
Al	1.858	1.781	1.839	1.961	1.676	1.240	1.130	1.208	1.232	1.139	4.944
Cr	0.001	0.009	0.040	0.004	-	0.003	0.001	-	0.001	-	0.009
Fe	2.444	2.391	2.387	2.500	2.328	2.251	0.006	0.002	0.004	0.003	5.011
Mn	0.047	0.046	0.046	0.039	0.040	0.042	-	0.001	-	0.001	0.035
Ca	1.737	1.724	1.723	1.773	1.765	1.728	0.211	0.212	0.303	0.016	0.036
Mg	2.185	2.239	2.207	2.099	2.374	2.563	-	-	-	0.002	4.023
K	0.063	0.061	0.063	0.068	0.053	0.041	0.003	0.006	0.004	0.660	0.008
Na	0.438	0.432	0.439	0.468	0.370	0.277	0.586	0.774	0.803	0.193	-
Total	15.547	15.518	15.527	15.598	15.491	15.344	4.763	4.994	5.117	4.936	19.797
X_{Fe}	0.528	0.516	0.520	0.544	0.495	0.468					0.555
X_{Ab}							0.733	0.780	0.723	0.222	
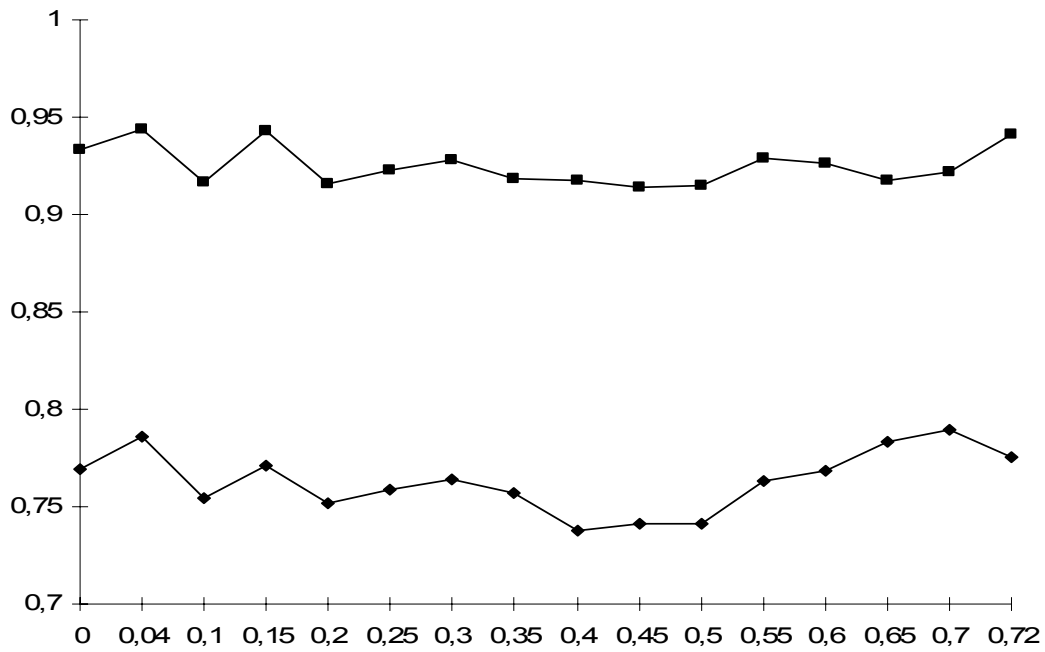
a
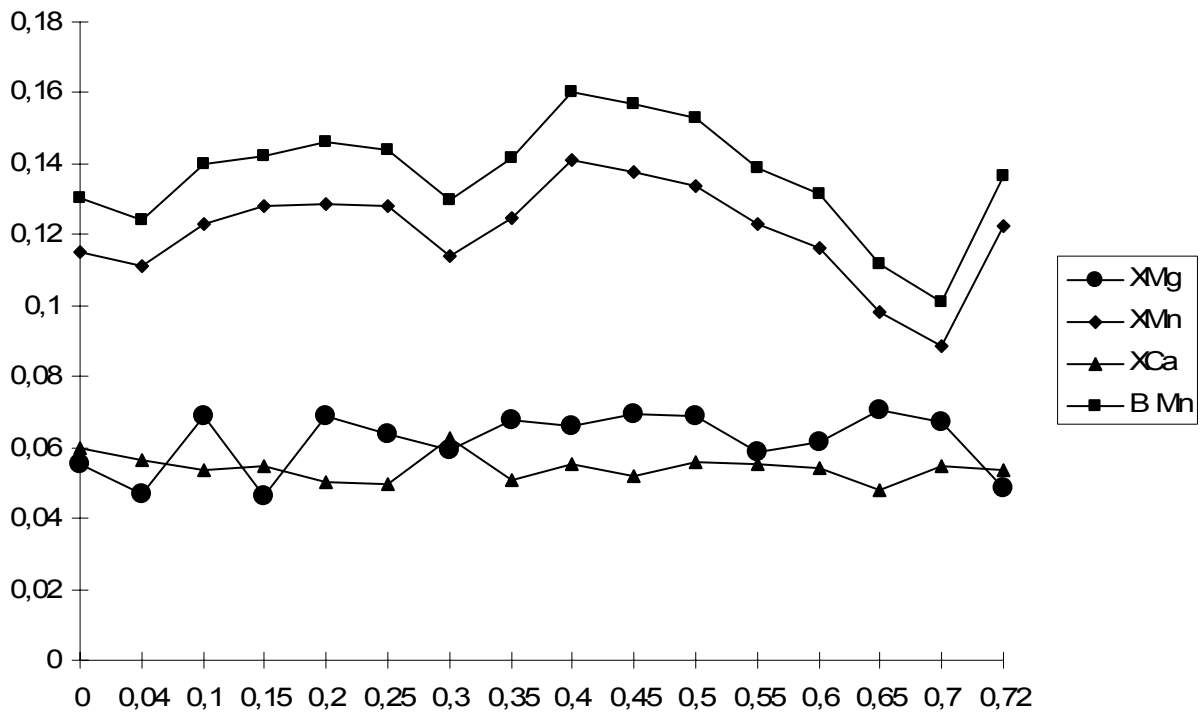
b

Figure A.2-8 a) AFe (top) and XFe for garnet 6, Kid 6; b) Graph showing the trends of BMn, XMn, XCa and XMg (from top to bottom) for garnet 6, sample Kid 6.
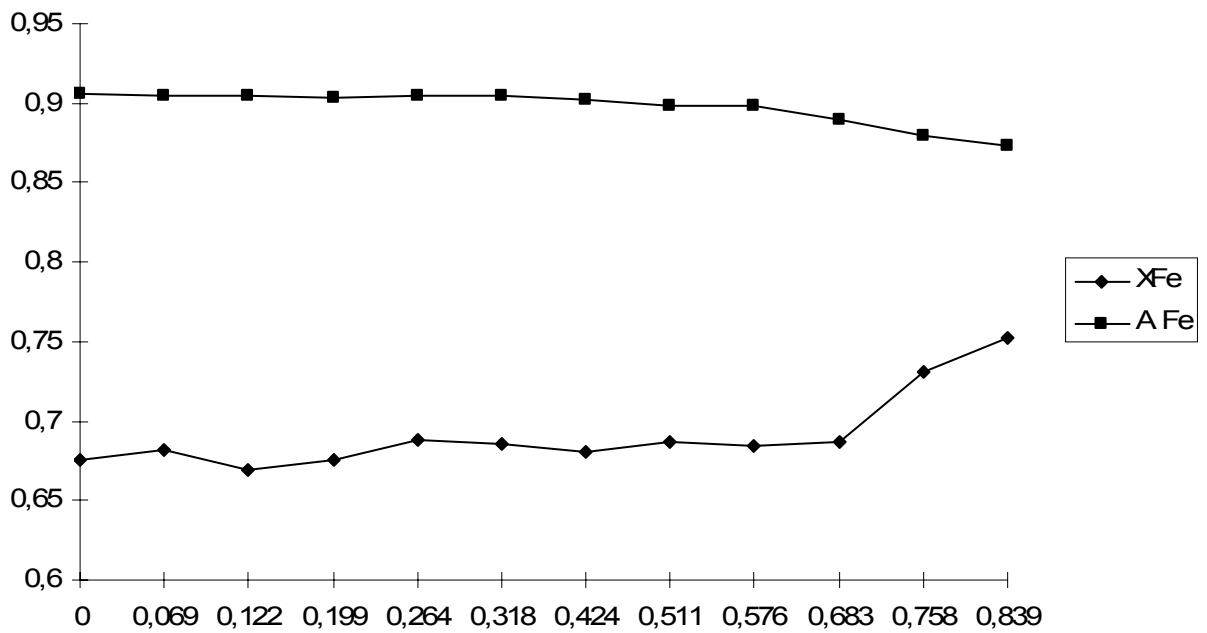
a
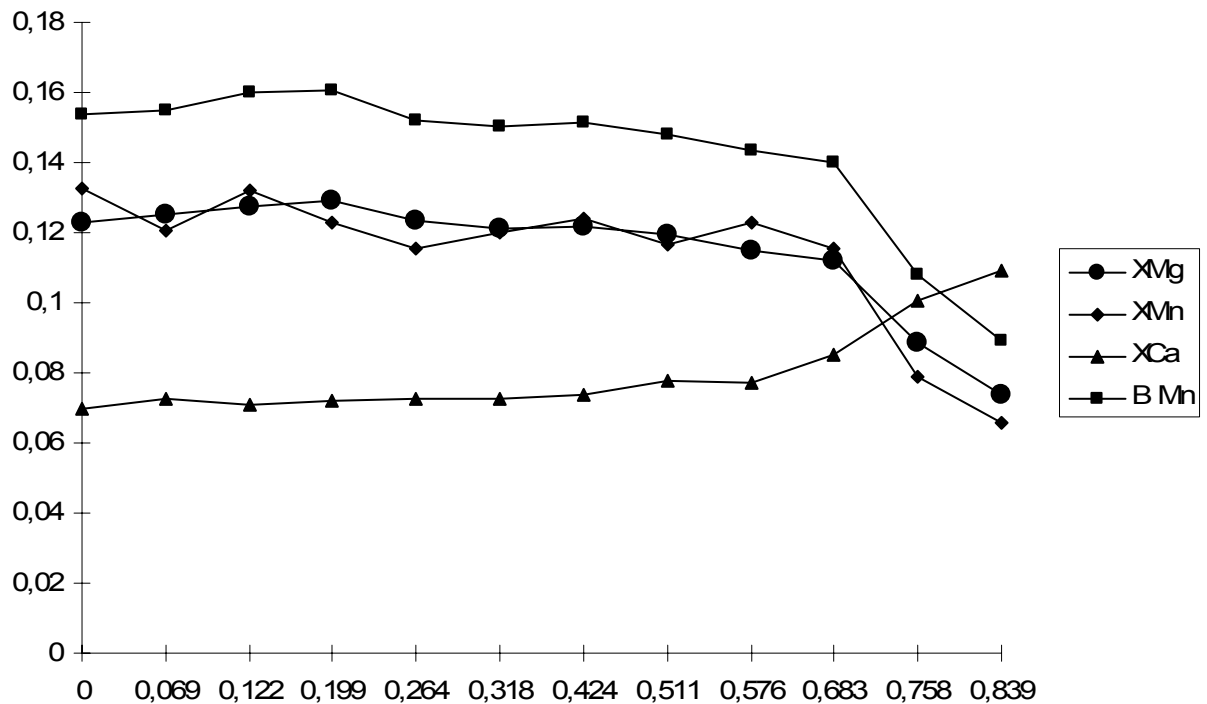
b

Figure A.2-9 a) Graph of AFe (upper line) and XFe, garnet 2, sample Kid 2; b) Graph showing trends of BMn (upper line), XMn, XMg and XCa (lowest line), garnet 2, Kid 2.

A.2.5.4 Discussion of PT results

Geothermobarometry indicates a low-pressure/high-temperature amphibolite facies metamorphism during the M_2 phase in the lower crustal rocks of the Wadi Kid area. Furthermore, the geothermobarometric results show an increase in pressure and temperature from south to north. These results are supported by the petrology of the rocks in the Wadi Kid area.

Garnet rims represent peak temperatures in the Wadi Kid and Wadi Lig, where the cores give the lower temperatures (Table A.2-8). Garnet zoning is the result of prograde metamorphism, i.e. the rims are enriched in almandine and pyrope and cores are enriched in spessartine and grossular (Figures A.2-6 to A.2-9). The zoning is suggested to be the effect of continuous garnet growth during prograde metamorphism. Garnets experienced minor effects of retrograde re-equilibration, as displayed by the decreasing almandine ratio close to the rim and so actual peak temperatures have been slightly higher than shown by our analytical results. Garnet core pressures have not been calculated in this study, due to the fact that the garnet cores are not in equilibrium with three other phases (muscovite, feldspar and biotite) in the rock.

The chemical composition of the amphiboles will give reliable information on the temperatures and pressures (Laird and Albee, 1981). Consequently thermobarometry of the mafic schists of the Malhaq Fm. (Table A.2-10) were used to give additional information on the P-T conditions in the Wadi Kid area because. The pressure used for the calculations was 4 kbar. Geothermometric results of the mafic schists in the Wadi Lig are consistent with the results of geothermometry with the Kleemann and Reinhardt geothermometer (1994) on the pelitic schists (sample B63).

Error estimation on the results of geothermobarometry is essential to reveal the consistency and quality of the results. Standard deviations from the results on the samples of the Wadi Kid and the Wadi Lig (Figure A.2-1) are all less than 50 °C, which is a common standard deviation for geothermometers. Most geobarometers have a standard deviation of 1 kbar. In this study, all standard deviations on the results are less than 1 kbar. The fact that the standard deviations in this study fall within the limits set by the authors of the calibrations used, is a measure for the consistency of our results.

Barrovian as well as Buchan zone metamorphic assemblages are found in the pelitic schists of the Wadi Kid area. The Buchan type Andalusite zone does not contain garnet or staurolite and the Barrovian type Staurolite zone does not contain andalusite. The overall presence of low pressure metamorphic assemblages, such as cordierite, andalusite and sillimanite, and the absence of blueschist facies rocks and kyanite gives rise to the conclusion that staurolite is not the relict of an earlier higher pressure metamorphic phase, but the product of prograde metamorphism.

Differences in temperatures and pressures are noticed when comparing the geothermobarometric results with the petrogenetic grid. Temperatures for the garnet-andalusite-biotite schist of the Malhaq Fm. are lower than the temperature range as predicted by the petrogenetic grid. The calculated pressures are generally more than 1 kbar higher then the pressures read from the petrogenetic grid. Calculated temperatures for garnet-andalusite-biotite-staurolite schist (Umm Zariq Fm.) equal the temperatures from the petrogenetic grid, the

Table A.2-8: P-T results for the pelitic schists of the central Wadi Kid. Bio-gt geothermometry (Kleemann & Reinhardt, 1994) and plag-bio-gt-musc geobarometry (Powell & Holland, 1988). Errors are mean deviations of the reported results.

Sample #	Core T (°C)	Rim T (°C)	P (kbar)
Kid 18			
G1	536	566	4.28
G2	533	559	3.98
G3	530	573	3.97
G4	504	578	4.23
G5	535	571	4.02
G6	527	565	3.98
G7	516	576	4.18
G8	528	550	3.81
Average	526±11	567±9	4.06±0.16
Kid 2			
G1	527	553	-
G2	526	562	-
Average	527±1	558±6	
Kid 6			
G1	505	545	3.45
G3	505	535	3.42
G4	506	546	3.48
G5	519	533	3.50
G6	488	539	3.48
Average	505±11	540±6	3.54±0.17

Table A.2-9: P-T results for the pelitic schists of the northern Wadi Kid. Bio-gt geothermometry (Kleemann & Reinhardt, 1994) and plag-bio-gt-musc geobarometry (Powell & Holland, 1988). Errors are mean deviations of

Sample #	Core T (°C)	Rim T (°C)	P (kbar)
B 63			
G1	590	620	4.16
G2	587	604	4.01
G3	-	626	4.20
Average	589±2	617±11	4.12±0.10

Table A.2-10: Temperature results for the Wadi Lig mafic schists (Holland & Blundy (1994)) thermometer, P = 4 kbar. Errors are mean deviations of the reported results.

Sample #	T (ed-tr)	T (ed-ri)	Average
WJ 61(n=15)	684±18	672±13	678±17
B 61 (n=36)	623±22	565±21	594±36
B64 (n=22)	668±18	594±13	631±41

difference between the pressures is 0.5 kbar. The calculated temperatures for the garnet-biotite assemblages (Malhaq and Umm Zariq Fm.) are within the stability field of the petrogenetic grid. Calculated pressures are higher than the pressures predicted by the petrogenetic grid.

Differences between the calculated pressures and temperatures and the PT-space for the stable assemblages on the petrogenetic grid can be explained by the errors involved in estimating pressures and temperatures. Secondly the behavior of natural assemblages differs from an ideal chemical system as is the Spear and Cheny (1989) grid. Thirdly the presence of small quantities of stabilizing elements, like MnO, extends the stability field of the phases present in the rock (Mahar et al, 1997 and Symmes and Ferry, 1992).

A.2.6 Evidence from PT-data for a core complex in the Wadi Kid Area

Blasband et al. (1997, 2000) have postulated, mainly on the basis of their structural data, that the Wadi Kid area represents a typical core complex. However to accept such an idea, evidence from geothermobarometry is crucial.

Metamorphic core complexes in extensional setting are characterized by LP/HT metamorphism in their lower crustal sequence due to the intrusion of granitoids into thinned crust (Gans et al, 1989; Lister and Baldwin, 1993). Pressures of metamorphism are less than or
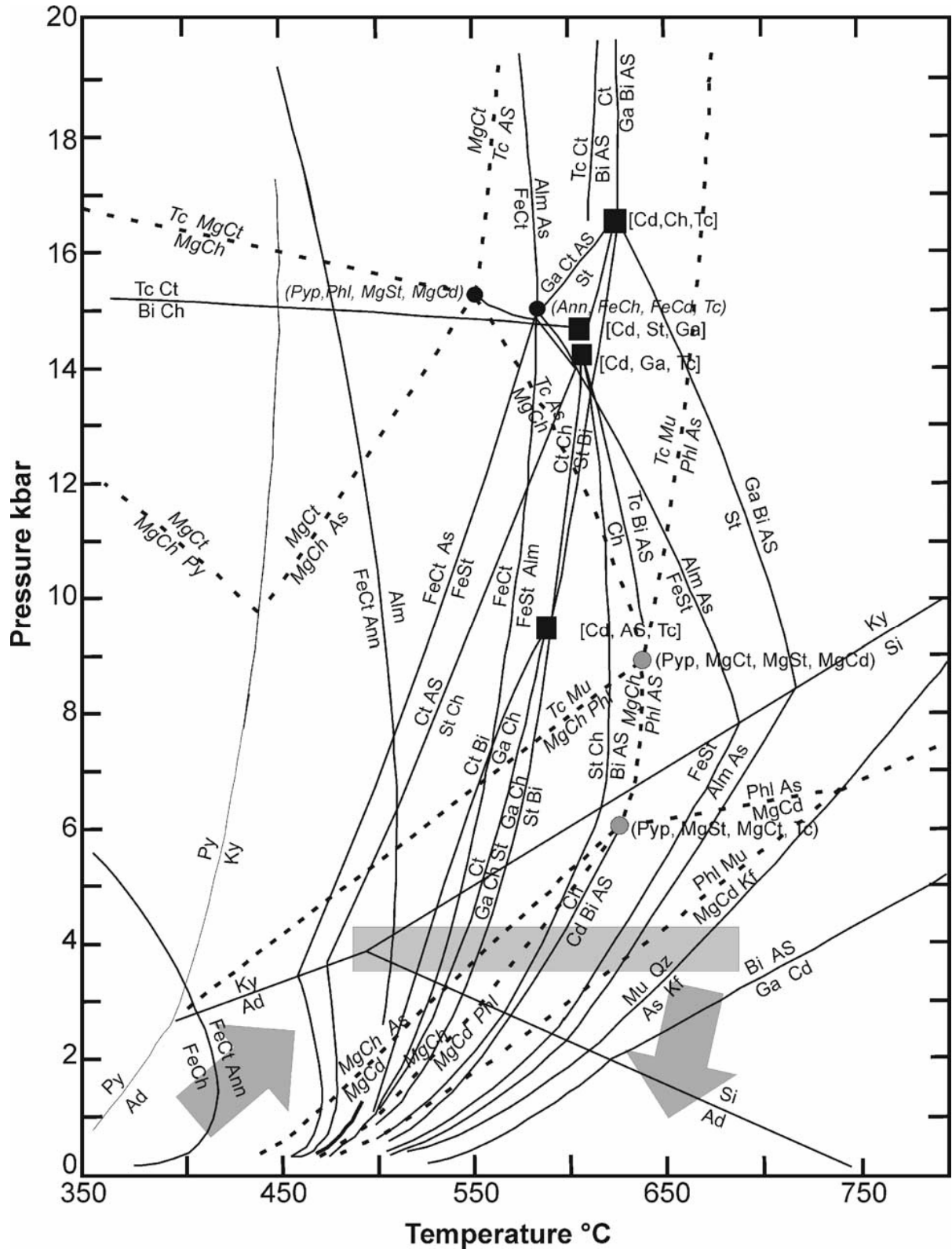
Figure A.2-10 Petrogenetic grid for the KFMASH system after Spear and Cheney (1989). The grey square defines the PT-space for the samples of the Wadi Kid area resulting from geothermobarometry. The arrows indicate the PTt-path during the M₁ and uplift phase.

equal to that of the aluminosilicate triple point and the temperatures range from 500-750°C (De Yoreo et al., 1991). Inferred pressure-temperature-time-paths (PTt-paths) are nearly isobaric in the early stages and turn clockwise during the later stages of uplift (De Yoreo et al., 1991). Metamorphic thermal gradients are generally higher than 40°C/km (Thompson, 1989; Barton, 1990). Evidence for isobaric PT-paths are found in garnets and peak temperatures are best represented by garnet rim compositions (Spear, 1991; Buick and Holland, 1989; House et al., 1997). Geothermochronological studies have shown that uplift of core complexes can be very rapid (Davis and Lister, 1988).

Davis (1980, 1987) has shown that there is a difference in structural styles between the upper and lower crustal rocks. Deformation in the upper-crustal rocks is brittle, while lower crustal rocks display ductile deformation. This implies a metamorphic break between the lower and the upper crustal rocks.

Metamorphism in the lower crustal rocks of the Wadi Kid area during M_2 is of the LP/HT-type. Temperatures range from 488 °C in the south to 684 °C in the north and pressures are in the range 3.4 to 4.28 kbar from south to north. Garnet rims define peak temperatures. Metamorphic thermal gradients are in the range 42-50 °C/km (assuming 1 kbar = 3.5 km). Metamorphism is prograde (see Figure A.2-10) as shown by the chemical trends in garnet.

The succession of andalusite after garnet can be observed in the Wadi Kid area. This is interpreted as a result of isothermal decompression (Gibson, 1992). Garnets show small retrograde rims (Figures A.2-6 to A.2-9). Retrograde rims on other metamorphic minerals are absent. These observations lead us to the conclusion that the uplift and cooling rates were relatively rapid.

The data on the metamorphic conditions presented above support the extensional core complex model of Blasband et al. (1997). Metamorphism during M_2 is charackterized by low-presssure/high-temperature conditions. The granitoids responsible for heating are the undeformed A-type granites and a non-deformed hornblende diorite in the northern Wadi Kid area. A mantle source is inferred for the hornblende diorite (Moghazi et al., 1998) and thus possibly indicates intrusion into a thinned crust. It is near the hornblende diorite that we found the highest temperatures (sample WJ 61, 687 °C) and thus it may be assumed that the hornblende diorite is the deepest-seated intrusion in the Wadi Kid area.

The upper crustal greenschist facies rocks of the M_1 phase are probably relicts of the arc-accretion phase (Blasband et al., 2000). These authors believe this phase to be responsible for the crustal thickening, which preceded the extensional collapse. The closure of the Mozambique Ocean resulted in arc-accretion and consequently the lithospheric thickening. (Blasband et al., 2000). This collisional phase is generally referred to as the East African Orogen. The M_1 metamorphic phase reflects metamorphism during this orogen. During the collapse stage, extensional core complexes were able to develop where LP/HT metamorphism took place as is observed during the M_2 phase in the Wadi Kid area. Blasband et al. (2000) postulated that the Late Proterozoic extensional phase in the Sinai, in which the core complex was formed, was due to the collapse of a compressed and thickened lithosphere. The HT/LP metamorphism as observed in the Wadi Kid area is a result of the very latest stage of the Late Proterozoic in the Middle East when collapse of this orogen led to extension and core complex formation

(Blasband et al. 2000).

A.2.7 Conclusions

1. Thermobarometry of metamorphic rocks from the Wadi Kid area reveal upper-greenschist to lower-amphibolite facies conditions of the LP/HT-type for the M_2 phase. Peak temperatures and pressures in the Wadi Lig also indicate LP/HT amphibolite facies conditions (687 °C and 4.28 kbar).
2. In the Wadi Kid area, a temperature increase is observed from south to north with highest temperatures recorded adjacent to the Sharira diorite.
3. Garnets show a progressive growth history and peak temperatures are given by garnet rim compositions.
4. M_2 metamorphism is associated with regional extension and the subsequent intrusion of granitoids.
5. The geothermobarometric results of this study support the core complex model, which is a result of collapse of the East African Orogen (Blasband et al., 1997; 2000).

Acknowledgements